INSTALAŢIE EXPERIMENTALĂ PENTRU MĂSURAREA CONCENTRAŢIEI DE OXIGEN DIZOLVAT ÎN APĂ

Nicolae BĂRAN[1], Gabriela MATEESCU[1] , Alexandru S. PĂTULEA[1]

[1]UNIVERSITATEA POLITEHNICA,Bucureşti, România.

Rezumat. În această lucrare autori prezintă cercetările experimentale privind determinarea concentraţiei de oxigen dizolvat în apă. Lucrarea prezintă o instalaţie experimentală pentru studiul oxigenării apei care cuprinde un rezervor paralelipipedic în interiorul căruia se află un generator de bule fine cu orificii de 0,3mm; înălţimea stratului de apă aflat deasupra generatorului este de 500mm. Conţinutul de oxigen dizolvat în apă se măsoară folosind un oxigenometru portabil şi se stabileşte dependenţa dintre concentraţia oxigenului dizolvat şi timpul de funcţionare al generatorului de bule fine. Se determină randamentul oxigenării şi eficienţa oxigenării apei. Lucrarea oferă o analiza a procesului de transfer a oxigenului din aer în apă prin evidenţierea factorilor care influenţează acest proces.
Cuvinte cheie: generator de bule fine, oxigenometru, oxigen dizolvat.

Abstract. The paper presents an experimental plant developed for the study of water oxygenation. The plant comprises a parallelepiped tank that contains inside a fine bubble generator; the water layer above the generator heights 500mm H_2O. The concentration of the oxygen dissolved in water is measured with an oxygen meter. The values are used in order to establish the dependency between the concentration of the oxygen dissolved in water and the functioning time of the fine bubble generator. The performance and the efficiency of water oxygenation are computed.
Keywords: fine bubble generator, oxygen meter.

1. INTRODUCERE

Procesele de oxigenare a apelor se întâlnesc în staţiile de tratare şi epurare a apelor reziduale, în industria alimentară, piscicultură şi chimie.

Oxigenul dizolvat în apă este cunoscut ca oxigen dizolvat (*fig.1.)* şi se măsoară convenţional în miligram de oxigen/litru.

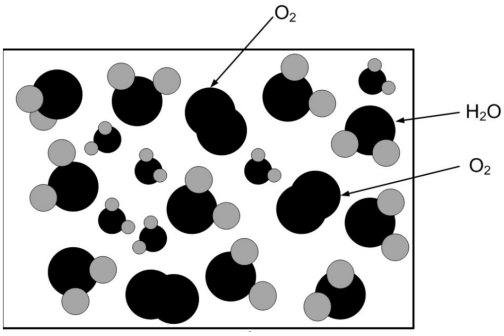

Fig. 1. Vedere a structurii moleculare: oxigen dizolvat apă

Din figura 1 se observă că: fiecare moleculă de apă este constituită dintr-o moleculă de oxigen de care sunt legate două molecule de hidrogen (o sferă neagră cuplată cu două sfere albe), între moleculele de apă, există molecule de oxigen (sfere negre) care constitue oxigenul dizolvat [1].

Cantitatea maximă de oxigen care poate fi dizolvat (absorbit în apă) depinde de mai mulţi factori fizico-chimici [1]:

1) – Presiunea atmosferică sau presiunea exercitată asupra apei;
2) – Temperatura apei;
3) – Salinitatea apei (cantitatea de săruri existentă în apă);
4) – Claritatea apei.

Un factor important este temperatura apei; cu cât apa este mai caldă cu atât mai putin oxigen dizolvat va exista în apă.

Astfel : la $t=10^oC$ apa proaspătă poate absorbi până la $11,3\ mgO_2/l$; la $t=25^oC$ se absoarbe numai $8,3\ mgO_2/l$;

Factorii care conduc la scăderea oxigenului dizolvat în apă sunt: temperatura crescută a apei; presiune scăzută asupra apei; poluarea apei cu petrol, ulei, detergenţi; prezenţa gheţii; adâncimea apei; turbiditate mare.

Măsurarea conţinutului de oxigen dizolvat în apă se poate face prin mai multe metode:

a) Metode chimice;

b) Metode electrice;
c) Metode optice.

Se prezintă pe scurt una din metodele electrice de măsurare a conţinutului de oxigen dizolvat în apă.

2. METODA ELECTRICĂ DE MĂSURARE A CONCENTRAŢIEI DE O_2 DIZOLVAT ÎN APĂ

Metoda electrică cunoscută şi sub numele de metoda electrochimică are la bază două tehnici pentru măsurarea concentraţiei de oxigen dizolvat în apă:

a) Tehnica procedeului galvanic, la care între electrozi avem o tensiune electrică foarte mică, nu este necesar aplicarea unei tensiuni electrice din exterior.

b) Tehnica procedeului polarografic, în cadrul căruia se aplică o tensiune electrică (curent continuu) între cei doi electrozi (catod şi anod).

Pentru efectuarea cercetărilor experimentale privind concentraţia oxigenului dizolvat în apă s-a achiziţionat un oxigenometru de la firma *HANNA INSTRUMENTS* – Canada tip *HI 9146* ce foloseste ca tehnică de măsurare procedeul polarografic. Aparatul se compune dintr-un microprocesor (*1*) (*fig.2*) care prin cablul de legătură (*2*) stabileşte legătura cu sonda de măsură (*3*). Sonda este formată dintr-un corp tubular ce defineşte un spaţiu închis cu un capac, acesta conţine o tijă izolată susţinută coaxial în interiorul camerei la partea superioară de o garnitură. La partea inferioară a tijei se află catodul ce este conectat la microprocesor print-un fir ce trece prin interiorul tijei, confecţionat dintr-un material special. Suprafaţa inferioară a tijei este acoperită cu un strat de material, conductor de electricitate ce formează anodul, la care este conectat firul către microprocesor. În porţiunea filetată se înşurubează un mic cilindru (*4*) care conţine o soluţie de electrolit (*6*). Baza cilindrului este constituită din o membrană de teflon (*5*) care este permeabilă pentru oxigen.

Fig. 2. Vedere de ansamblu a oxigenometrului pregătit pentru măsurători.

1-microprocesor; 2-cablu de legătură; 3-corpul sondei; 4-mic cilindru ce conţine o soluţie de electrolit; 5-membrană de teflon permeabilă la oxigen; 6-fiolă cu soluţie

Principiul de funcţionare al aparatului este următorul: în interiorul microprocesorului (*1*) se află o baterie de alimentare în curent continuu şi astfel în sondă între electrozi se stabileşte un câmp electric în care migrează ionii.

Între electrozi (anod şi catod) se află o soluţie de electrolit specială conţinută într-un mic tub cilindric (*4*) izolat faţă de apă. Tubul cilindric este prevăzut cu o membrană din teflon (*5*) permeabilă la oxigenul dizolvat în apă.

Oxigenul care străbate membrana reacţionează la catod şi determină o modificare a curentului în circuitul catod-anod din interiorul electrolitului. Sonda transmite această modificare a curentului la microprocesor, modificare proporţională cu cantitatea de oxigen (O_2) care a pătruns prin difuziune prin membrană şi a reacţionat la catod. Pe ecranul microprocesorului apare concentraţia de O_2 [*mg/l*] şi temperatura apei.

3. SCHIŢA INSTALAŢIEI

După procurarea oxigenometrului de la firma *HANNA INSTRUMENTS* am constatat faptul că în prospect se cerea ca pentru măsurători exacte apa trebuie să curgă cu o viteză mai mare de *0,3m/s*. Acest lucru în laborator conduce la un mare consum de apă şi am stabilit să deplasăm sonda cu o viteză:

$$v = \frac{S}{\tau} = \frac{\pi d}{\tau} \qquad (1)$$

unde:

d – diametrul cercului pe care se deplasează sonda aflat la mijlocul distanţei dintre peretele rezervorului şi axa rezervorului, $d=0,25m$;

τ – timpul în care sonda efectueză o rotaţie completă; $\tau=2s$.

v – viteza de deplasare a sondei:

$$v = \frac{\pi \cdot 0,25}{2} = 0,3925 m/s \qquad (2)$$

Instalaţia experimentală (*fig.3*) cuprinde:

a) Un rezervor din pexiglas transparent de formă paralelipipedică cu volumul: $0,5\times0,5\times1,6=0,4m^3$;

b) O conductă de aer comprimat care alimentează generatorul de bule fine(G.B.F);

c) Dispozitiv de antrenare în mişcare circulară a sondei de măsură a concentraţiei de oxigen dizolvat în apă;

d) Cablu de legătură de la sondă la oxigenometru;

e) Oxigenometru tip *HI 9146*;

f) Aparate de măsură privind aerul insuflat în rezervor:

- Rotametru pentru măsurarea debitului de aer;
- Manometru digital pentru măsurarea presiunii aerului;
- Termometru digital pentru măsurarea temperaturii aerului.

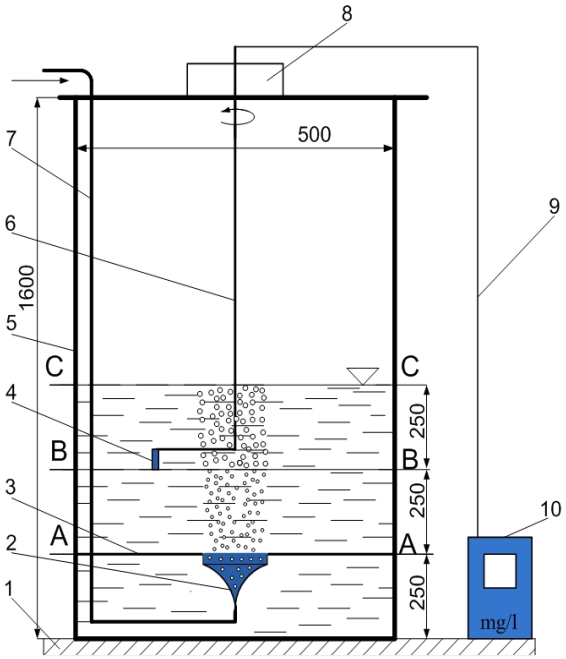

Fig. 3. Schiţa generală a instalaţiei experimentale
1 - placa de bază; 2 - generator de bule fine; 3 - placă de separare; 4 - sonda oxigenometrului; 5- rezervor din pexiglas transparent; 6 - tijă de acţionare a sondei oxigenometrului; 7 - conductă de alimentare cu aer comprimat; 8 - dispozitiv de acţionare a tijei; 9 - cablu de legătură între sondă şi oxigenometru;10 - oxigenometru.

În figura 3 placa de separaţie (*3*) separă un strat de apă de *h=250mm* (aflat sub nivelul generatorului de bule fine) de volumul de apă supus oxigenării.

Acest fapt este similar cu amplasarea unor generatoare de bule fine pe fundul unui bazin în care are loc aerarea (oxigenarea) apelor uzate.

Pentru efectuarea măsurătorilor privind concentraţia de O_2 am ales următoarea soluţie:

Cu ajutorul dispozitivului de acţionare, sonda oxigenometrului va fi deplasată pe un cerc cu diametrul de *250mm* (*fig.4*).

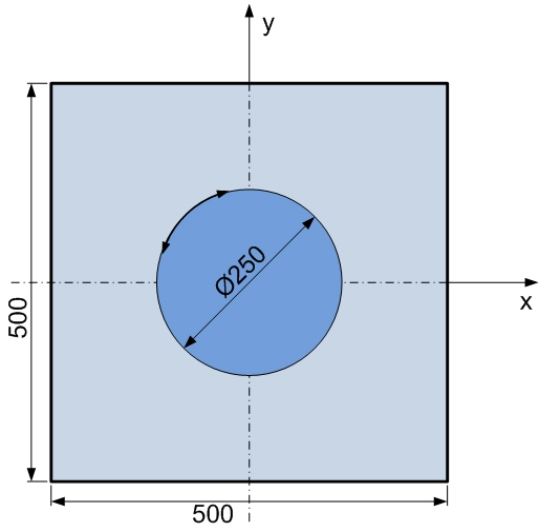

Fig. 4. Traseul parcurs de sonda de măsură, într-o secţiune transversală a rezervorului cu apă

Se precizează că măsurătorile se efectuează după ce generatorul de bule fine, (după un timp de funcţionare) a fost oprit.

4. METODICA MĂSURĂTORILOR

- Înainte de efectuarea oxigenări propriu zise se măsoară concentraţia de O_2 dizolvat, rezultată în urma oxigenări mecanice (barbotare) prin umplerea bazinului cu apă şi a concentraţiei iniţiale de oxigen dizolvat deja existentă în apa de la reţea.
- G.B.F. are o poziţie fixă în secţiunea A-A iar măsurarea concentraţiei de oxigen dizolvat în apă se efectuează în secţiunea B-B, la mijlocul stratului de apă.
- În timpul măsurătorilor se va măsura presiunea aerului comprimat şi debitul de aer valori care vor fi menţinute constante în timp.

În instalaţia experimentală deasupra plăcii perforate se află un strat de apă de înălţime $H=500mmH_2O$, iar presiunea datorită tensiunii superficiale [2] este :

$$p_{ts} = \frac{2\sigma}{r_0} = \frac{2 \cdot 8 \cdot 10^{-2}}{0,25 \cdot 10^{-3}} = 620 N/m^2 \qquad (3)$$

$$\Delta h_{ts} = \frac{p_{ts}}{\rho_{H2O} \cdot g} = \frac{620}{10^3 \cdot 9,81} = 0,063 mH_2O \qquad (4)$$

Ca urmare, primele bule de gaz vor apărea dacă manometrul digital va arăta:

$$\Delta h_1 > H + \Delta h_{ts} \Rightarrow \Delta h_1 > 563 mmH_2O \qquad (5)$$

Fig. 5. GBF în funcţiune; Δh_1=60mbar=611mmH_2O

În cercetările anterioare [3][4], s-a stabilit că presiunea aerului la intrarea în G.B.F. să fie de *611mmH_2O>563mmH_2O* deci G.B.F. (fig.5) funcţionează normal.

Măsurătorile se vor efectua în patru etape.

I) La prima etapă de măsurători, situaţia se prezintă în figura 5, unde stratul de apă de apă aflat deasupra GBF este de h_{H2O}*=500mm* , sonda este la $h_{sondă}$*=250mm* , concentraţia de oxigen dizolvat iniţială fiind c_0 *=5,12mg/l* iar indicaţia contorului electric este E_0=31,6kWh şi temperatura apei este de *t=19,5°C*.

Se măsoară presiunea şi debitul de aer care pătrunde în G.B.F.: p_1*=611mmH_2O ;* $\dot{V}_1 = 540 l/h$; valori care se menţin constante în timpul măsurătorilor.

După un timp $\Delta\tau_1$*=15'* de funcţionare a G.B.F. se întrerupe funcţionarea G.B.F. şi se măsoară concentraţia de O_2 prin rotirea sondei în apă în secţiunea B-B (*fig.3*).

II) Se pune în funcţiune G.B.F. şi se introduce aer în apă timp de *15'* ajungându-se la un timp total de $\Delta\tau_2$*=30' ;* se măsoară concentraţia de O_2 în secţiunea B-B.

III) Similar se ajunge la $\Delta\tau_3$*=45'*.

IV) Similar se ajunge la $\Delta\tau_4$*=60'*.

În final se măsoară concentraţia de O_2 dizolvat în apă după o oră de funcţionare a G.B.F. valorile mărimilor măsurate sunt date în tabelul I.

Tabel I
Variaţia concentraţiei de O_2 în funcţie de timpul cât a funcţionat G.B.F.

τ=0'	τ=15'	τ=30'	τ=45'	τ=60'
5,12	6,57	7,16	7,63	7,97

Pe baza datelor din tabelul I se construieşte graficul $C_{O_2} = f(\tau)$ pentru secţiunea B-B în cazul când înălţimea stratului de apă este *500mmH_2O* şi $t_{H_2O} = 19{,}5^o C$

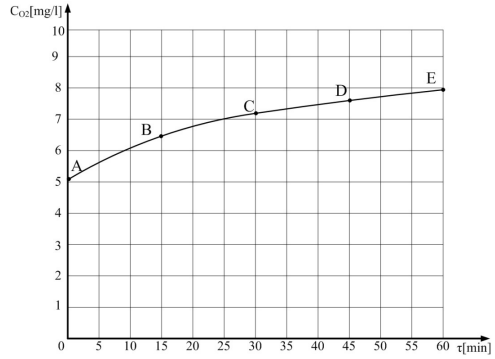

Fig.6 . Variaţia concentraţiei de oxigen dizolvat în apă în funcţie de timp pentru secţiunea B-B

Punctul A reprezintă concentraţia de O_2 dizolvat în apă la începutul măsurătorilor; punctul B ne indică concentraţia de O_2 dizolvat în apă după ce GBF a funcţionat *15`*, punctul C după *30`*, punctul D după *45`* şi punctul E după *60`*.

Oxigenul transferat în apa curată (apă de la reţea) nu a fost consumat în cadrul metabolismului microorganismelor (vezi reactoare, staţii de tratare a apelor) şi nici de către peşti, ca urmare concentraţia de oxigen în apă a crescut pe măsură ce a fost insuflat aer în rezervorul cu apă.

5. DETERMINAREA RANDAMENTULUI PROCESULUI DE OXIGENARE SI A EFICIENTEI AERARII

Se evidenţiază următoarele aspecte:

1. Randamentul oxigenării apei este definit ca raportul dintre oxigenul dizolvat în apă şi oxigenul introdus în apă [5]:

$$\eta_{ox} = \frac{\dot{V}}{\dot{m}_{O_2}} \frac{dC}{d\tau} = \frac{\dot{V}}{\rho_{O_2} \dot{V}_{O_2}} \cdot aK_l (C_s - C) \qquad (6)$$

Relaţie în care:

V – volumul apei supusă oxigenării [m^3];

$\dot{m}_{O_2}$ – debitul de oxigen introdus în apă [*kg/s*];

$\frac{dC}{d\tau}$ – viteza de transfer a oxigenului dizolvat [$kg/m^3 \bullet s^{-1}$]

aK_l – coeficient volumetric de transfer de masă [*1/s*];

C_s – concentraţia masică a componentului transferabil la saturaţie (la echilibru) în faza lichidă [kg/m^3];

C – concentraţia masică curentă a componentului transferabil în faza lichidă [kg/m^3].

Randamentul oxigenării se poate stabili în două situaţii:

I) În regim staţionar, adică cât oxigen se introduce în rezervor, este consumat de peşti şi alte vieţuitoare prezente în apă, în acest caz: $\frac{dC}{d\tau} = ct$, viteza de transfer a oxigenului dizolvat este constantă.

Matematic dependenţa concentraţiei de O_2 dizolvat în funcţie de timp, prezentată în figura 6 are un singur punct în care este valabilă de exemplu:

$$\left(\frac{dC}{d\tau}\right)_B = \frac{\Delta C}{\Delta \tau} = ct \tag{7}$$

Acestă valoare se menţine constantă în cazul regimului staţionar.

Deci în cazul regimului staţionar avem o valoare constantă a randamentului oxigenării.

II) În cazul regimului nestaţionar se introduce o cantitate de aer (deci şi O_2 *21%*) în timp.

Concentraţia de oxigen dizolvat în apă se modifică în timp, adică va creşte. Ca urmare graficul $C_{O_2} = f(\tau)$ va avea pante diferite.

Dacă se aleg patru puncte de măsură: $C_1 = f(\Delta\tau_1)$, $C_2 = f(\Delta\tau_2)$, $C_3 = f(\Delta\tau_3)$, $C_4 = f(\Delta\tau_4)$, înseamnă că vom obţine patru valori pentru randamentul oxigenării.

Panta între două puncte succesive :

$$\frac{\Delta C}{\Delta \tau} = \frac{C_{i+1} - C_1}{\tau_{i+1} - \tau_1} \tag{8}$$

Această valoare determinată experimental ne ajută să determinăm:

$$\frac{\Delta C}{\Delta \tau} = aK_l (C_s - C) \tag{9}$$

în care aK_l este dificil de stabilit.

Din graficul din figura 6 se calculează succesiv pentru zonele A-B, B-C, C-D, D-E:

$$\left(\frac{dc}{d\tau}\right)_{AB} = \frac{C_B - C_A}{\tau_B - \tau_A} = \frac{(6{,}57 - 5{,}12)[mg/l]}{15 \cdot 60[s]} = \\ = \frac{1{,}45 \cdot 10^{-3}[kg/m^3]}{900[s]} = 0{,}1611 \cdot 10^{-5}\left[\frac{kg}{m^3} \cdot \frac{1}{s}\right] \tag{10}$$

$$\left(\frac{dc}{d\tau}\right)_{BC} = \frac{C_C - C_B}{\tau_C - \tau_B} = \frac{(7{,}16 - 6{,}57)[mg/l]}{15 \cdot 60[s]} = \\ = 0{,}0656 \cdot 10^{-5}\left[\frac{kg}{m^3} \cdot \frac{1}{s}\right] \tag{11}$$

$$\left(\frac{dc}{d\tau}\right)_{CD} = \frac{C_D - C_C}{\tau_D - \tau_C} = \frac{(7{,}63 - 7{,}16)[mg/l]}{15 \cdot 60[s]} = \\ = 0{,}0522 \cdot 10^{-5}\left[\frac{kg}{m^3} \cdot \frac{1}{s}\right] \tag{12}$$

$$\left(\frac{dc}{d\tau}\right)_{DE} = \frac{C_E - C_D}{\tau_E - \tau_D} = \frac{(7{,}97 - 7{,}63)[mg/l]}{15 \cdot 60[s]} = \\ = 0{,}0378 \cdot 10^{-5}\left[\frac{kg}{m^3} \cdot \frac{1}{s}\right] \tag{13}$$

În cadrul regimului nestaţionar randamentul oxigenării pentru prima etapă de funcţionare va fi:

$$\eta_{ox} = \frac{V}{\dot{m}_{O_2}} \cdot \frac{dC}{d\tau} \tag{14}$$

V – volumul de apă supus procesului de oxigenare $V = 0{,}5 \times 0{,}5 \times 0{,}5 = 0{,}125 m^3$;

$\dot{m}_{O_2}$ – debitul de oxigen introdus în apă [*kg/s*];

Din literatura de specialitate [6][7] se cunoaşte:

$$\dot{m}_{O_2} = 0{,}233\ \% \dot{m}_{aer}[kg/s] \tag{15}$$

$$\dot{m}_{O_2} = \rho_{aer} \cdot \dot{V}_{aer} \tag{16}$$

$$\rho_{aer} = \frac{p_{aer}}{RT_{aer}} \tag{17}$$

Suprapresiunea aerului:

$$\Delta p_{aer} = 60 mbar = 60 \cdot 10^{-3} bar = \\ = 60 \cdot 10^{-3} \cdot 10^5 N/m^2 = 6000 N/m^2 \tag{18}$$

$$p = p_{atm} + \Delta p_{aer} = 101325 + 6000 = \\ = 107325 N/m^2 \tag{19}$$

$$T_{aer} = t_{o_C} + 273{,}15 = 22 + 273{,}5 = 295{,}15 K \tag{20}$$

$$R_{aer} = 287\, j/kgK \tag{21}$$

$$\rho_{aer} = \frac{107325}{287 \cdot 295.15} = 1{,}267 kg/m^3 \tag{22}$$

$$\dot{V}_{aer} = 540 l/h = \frac{540 \cdot 10^{-3}}{3600} = 15{,}0 \cdot 10^{-5}[m^3/s] \tag{23}$$

$$\dot{m}_{aer} = \rho_{aer} \cdot \dot{V}_{aer} = 1{,}267 \cdot 15{,}0 \cdot 10^{-5} = \\ = 0{,}19 \cdot 10^{-3} kg/s \tag{24}$$

$$\dot{m}_{O_2} = 0{,}23 \cdot \dot{m}_{aer} = 0{,}233 \cdot 0{,}19 \cdot 10^{-3} = \\ = 0{,}0437 \cdot 10^{-3} kg/s \tag{25}$$

$$\eta_{ox} = \frac{V}{\dot{m}_{O_2}} \cdot \frac{dC}{d\tau} = \frac{0,125}{0,0437 \cdot 10^{-3}} \cdot 0,1611 \cdot 10^{-5} = \\ = 0,46 \cdot 10^{-2} \quad (26)$$

2. Eficienţa oxigenării apei

Eficienţa aerării apei ne indică cantitatea de oxigen transferată apei pentru un consum de energie electrică; pentru prima etapă ($\Delta\tau_1 = 15'$) se obţine:

$$E = \frac{kgO_2}{kWh} = \frac{0,0437 \cdot 10^{-3} \cdot 900}{0,15} = \\ = 0,262[kgO_2 / kWh] \quad (27)$$

Din literatura de specialitate [5] în cazul oxigenării pentru apă pură la t=20°C se indică:

$$C_{O_2} = 2[mgO_2 / l], C_s = 9,02[mgO_2 / l] \quad (28)$$

$\eta_{ox} = 2,8h$ şi E=2,18 [kgO$_2$/kWh];
dacă $h = 3,5m$ $\eta_{ox} = 10\%$ (29)

În comparaţie cu datele existente în literatură pentru valorile obţinute experimental se poate concluziona:

a) În procesul de oxigenare intervin două mărimi esenţiale: înălţimea apei în bazin şi concentraţia iniţială a oxigenului dizolvat în apă.

Dacă în relaţia (10) se introduce C_{O_2} din relaţia (29) se obţine:

$$\left(\frac{dc}{d\tau}\right)_{AB} = \frac{(6,57 - 2.0)[mg / l]}{15 \cdot 60[s]} = \\ = 0,507 \cdot 10^{-5} \left[\frac{kg}{m^3} \cdot \frac{1}{s}\right] \quad (30)$$

Iar randamentul oxigenării va fi:

$$\eta_{ox} = \frac{V}{\dot{m}_{O_2}} \cdot \frac{dC}{d\tau} = \frac{0,125}{0,0437 \cdot 10^{-3}} \cdot 0,507 \cdot 10^{-5} = \\ = 1,45 \quad (31)$$

Această valoare este apropiată de cea care se obţine din relaţia (29):

$$\eta_{ox} = 2,8h = 2,8 \cdot 0,5 = 1,4 \quad (32)$$

b) Deci randamentul oxigenării şi eficienţa aerării în cazul cercetărilor experimentale sunt reduse deoarece concentraţia iniţială a oxigenului dizolvat este mare $(5,12 \leftrightarrow 2)$ iar înălţimea stratului de apă este mică $(0,5m \leftrightarrow 3,5m)$

6. CONCLUZII

1. Rezultatul cercetărilor experimentale vor oferi dezvoltarea de noi modele de calcul a variaţiei concentraţiei de oxigen dizolvat în apă.
2. Cercetările experimentale de laborator au fost efectuate într-un efort de a elucida mecanismul transferului de oxigen către apă cu suprafaţă liberă.
3. Soluţia originală pentru generatorul de bule fine realizat prin electroeroziune asigură o repartiţie uniformă a bulelor de aer în rezervorul de apă.
4. Metoda de măsură asigură o precizie sporită şi este uşor de utilizat.
5. Rezultatele cercetărilor viitoare vor oferi oportunitatea de a valida noi modele de G.B.F. care să ducă la îmbunătăţirea cantităţilor de oxigen dizolvat în apă, cu un consum de energie cât mai mic.
6. În urma cercetărilor experimentale se relevă faptul că asupra randamentului oxigenării apei o influenţă importantă o au concentraţia iniţială a oxigenului dizolvat şi înălţimea stratului de apă aflat deasupra G.B.F.
7. Cercetările vor continua în domeniul oxigenării apelor prin sprijinul unui Contract POSDRU/88/1.5/S/60203.

REFERINŢE

[1] Chris Wilson – *Note privind calitatea apei*, Departamentul de Ştiinţa Solului şi Apei. Universitatea din Florida, Florida (2010).

[2] Gh. Băran, N. Băran – *Hidrodinamica bulelor generate de difuzori poroşi*. Revista de Chimie ,vol. 54 , nr.5, pag.436-440, Bucuresti (2003)

[3] N.Baran, Gh. Băran, G.Mateeescu, Al.Pătulea – *Water oxygenation*. Buletinul Institului Politehnic din Iaşi tomLXI (LX) fasc.3b, Iaşi (2010).

[4] N. Băran, Gh. Băran, G. Mateescu, D. Besnea – *Experimental Research regarding a New Type of Fine Bubble Generator*. Romanian Review Precision Mechanics Optics and Mechatronics, ISSN 1584-5982, Bucureşti (2009).

[5] D. Robescu s.a. – *Fiabilitatea proceselor şi echipamentelor de tratare şi epurare a apelor*. Editura Tehnică, Bucureşti (2002)

[6] N. Băran, M. Marinescu, V. Radcenco, *Termodinamică tehnică vol I.II.III*. Editura MATRIXROM, Bucureşti (1998).

[7] Al.Dobrovicescu,N.Băran,ş.a. – *Elemente de Termodinamică Tehnică*. Editura POLITEHNICA PRESS ,Bucureşti (2009)

STUDIES OF A SYSTEM OF TEMPERATURE CONTROL WITHOUT THE CORRECTION CENTER

Adrian CERNĂIANU, Dragoş TUTUNEA , Eugenia STĂNCUŢ, Alexandru DIMA

UNIVERSITY OF CRAIOVA, Romania.

Rezumat. În lucrare se prezintă analiza influenţei fenomenelor termice apărute în procesul de rectificare fără centre cu avans transversal, în zona de contact dintre corpul abraziv aşchietor şi piesa prelucrată, care influenţează astfel atât precizia diemensională a piesei cât şi stabilitatea procesului, prin metodele analitice clasice cât şi prin metode moderne computaţionale folosind analizele termice cu elemente finite.
Cuvinte cheie: termic, căldură, rectificare, element finit, dilatare, control.

Abstract. The paper presents analysis of the thermal effects of cutting on parts processed without correction in the center, in contact area between abrasive disk cutting and work piece, influencing the accuracy in measurement and process stability. In work is use classical analytical methods and modern computational methods with finite element thermal analysis.
Keywords: thermal, heat, grinding, finite element, dilatation, control.

1. INTRODUCTION

It is known as, of grinding process, workpiece temperature increases and because of the high circumferential speed of the abrasive disk cutting can to achieve, locally, high values between 800 and 1000^0C.

Heat generated while grinding comes from the mechanical work by removing material part, from mechanical work of friction of the grinding wheel with part surface grinding and from the external environment.

By proceedings these three sources of heat establishes a variable thermal equilibrium and each part of the system machine-tool-part has his own temperature, different temperature of the other components. These differences of temperatures give rise measurement and processing errors.

Temperature part depends on the following factors:

- technological regime grinding;
- flow rate and temperature of coolant;
- variation machining allowance;
- frequency of straightening the abrasive disc cutting.

This phenomena, of transmission of heat from the cutting area is made naturally from body or within bodies, rom areas with high temperature to areas with lower temperature, with possibility of dilation of parts or elements work establishment, with negative influences on the processing accuracy.

1.1. Mechanical work and heat in the grinding process

To obtaining the precision of parts processing on centerless grinding machines with cross feed is the appearance of heat that accompanies constant process of cutting metals. Appearance of the heat source is the total work L, used in the cutting process and is given by:

$$L = L_1 + L_2 + L_3 + L_4 \qquad (1)$$

where: L_1 - the mechanical work of plastic deformation of metal removed in form of chips;

L_2 - mechanical work consumed by friction between the chip and grain of grinding;

L_3 - elastic deformations of mechanical work consumed;

L_4 - mechanical work consumed with friction between the grain and surface of grinding.

Mechanical work consumed in the cutting process is almost entirely converted into heat, which will be produced primarily in the cutting plane and in the secondly chip-friction areas and the area of grain and grain processing.

For these areas, heat is transmitted in areas with lower temperature, and is divided between chips Q1, Q2 abrasive disc grinding, blank Q3, Q4 coolant and environment Q5, so:

$$Q_1 + Q_2 + Q_3 + Q_4 + Q_5 = Q_d + Q_f \qquad (2)$$

where: Q_d- is the amount of heat generated by deformation;

Q_f - amount heat due to friction.

Phenomenon of heat due to the friction removing material was studied in a centerless grinding machine model with cross feed, designed, developed and tested by their own efforts.

Structural and technological elements of this model of tool can be seen in the image in Figures 1 and 2, and determining the value of the thermal field in the area of processing of samples was performed by using a powerful device for measuring the temperature with laser spot, class A, model RAY RPM, RAYTEC Inc.USA, as shown in the image of Fig. 3.

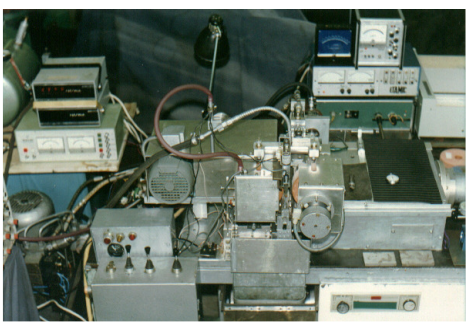

Fig. 1. Machine centerless grinding to advance cross

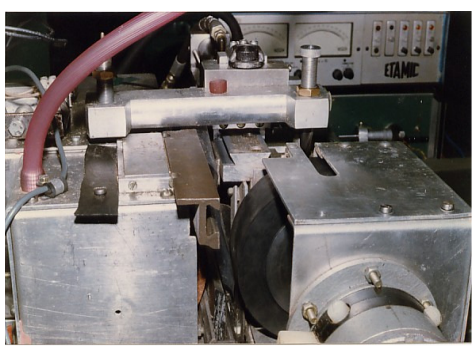

Fig. 2. Cutting area

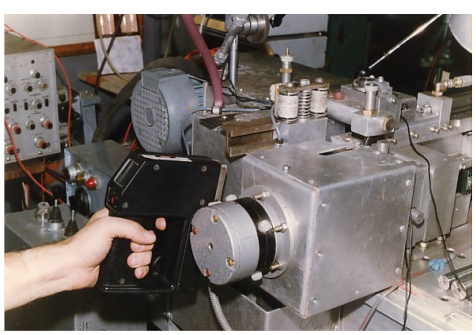

Fig. 3. Measurement of temperature in the cutting area

1.2. THE CALCULATION SPECIFIC HEAT ON THE WORKPIECE SURFACE

Complex thermodynamics phenomena occurring in this area, believing that the surface of the sample subject processing moving area of contact with the cutting abrasive disc that can go as far to 800-1000^{0}C (even 1100 ^{0}C). In this way layers appear affected by the thermal effect produced on the sample surface and until a depth where the temperature reaches up to 820-850 ^{0}C occurs oil hardening phase material and change its crystal structure.

Thus, most of the rectifying mechanical power turns into heat and only a few insignificant is transformed in energy change of lattice the workpiece material. Thermal energy is distributed among piece cutting abrasive disk, chips and coolant results as to the formula:

$$\frac{F_{aş} \cdot v_{aş}}{60 \cdot 75} = Q_p + Q_{da} + Q_a + Q_l + Q_r \qquad (3)$$

where: Q_p is heat taken of piece;

Q_{da} - heat taken from the cutting disk;

Q_a - heat taken from chip;

Q_l - heat taken from coolant;

Q_r - heat transferred by radiation of the environment.

Following the grinding is considered that only a small part of the heat radiation gives of the environment and about 80% passes in the part. This heat is an important factor in the process of correcting the changes could have on the superficial layer of the workpiece, and processing by direct action on the precision and quality parts.

The instantaneous temperature can cause changes in the composition of parts is difficult to measure and even numeracy tests give quite different results.

Heat transferred part during processing, satisfies the following relationship:

$$Q_p = 0,885 \cdot Q_{\max} \cdot B\sqrt{\lambda_p \cdot c_p \cdot \rho_p \cdot v_p \cdot L} \qquad (4)$$

where: $Q_{max.}$ is the maximum temperature in the processing area;

B - cutting abrasive disk width;

λ_p - coefficient of thermal conductivity of workpiece;

c_p - heat capacity of workpiece;

ρ_p - the density of part;

v_p - speed workpiece subjected processing;

L - length of arc contact.

Maximum temperature determines the thermal stability of the cutting process only if it has a lower value than the permissible temperature, which

depends, in its turn, to the maximum allowable working regime parameters (v, s, t) as relationship:

$$Q_{\max} = C_\theta \cdot v_{as}^{x_\theta} \cdot s_{av}^{y_\theta} \cdot t^{z_\theta} \cdot B^{p_\theta} \qquad (5)$$

in which: C_θ is a coefficient with values from 82.7 to 1398.5;

x_θ, y_θ, z_θ, p_θ are constants which depend on the characteristics of cutting abrasive disk and workpiece under the processing, with the following values: x_θ =0,3; y_θ=0,21; z_θ=0,52; p_θ=0,16.

Given the experimental values obtained from processing parts: $D_{aş}$ = 148 mm; D_p = 25,15 mm; $n_{aş}$ = 2956 rot/min; n_p =280 rot/min; $B_{aş}$ = 40 mm; B_p = 19,8 mm; L = 2,5 mm; s_{av} = 2,45 mm/min; t = $1{,}54 \cdot 10^{-3}$ mm/rot by coefficient values: λ_p = 43,2 W/mK; c_p = 470 J/kg K; ρ_p = 7790 kg/m^3, results:

$$Q_{\max} = (82{,}7 \div 1389{,}5) \cdot \left(\frac{\pi \cdot 148 \cdot 2956}{1000}\right)^{0,3} \cdot$$

$$\cdot 2{,}45^{0,21} \cdot \left(1{,}54 \cdot 10^{-3}\right)^{0,52} \cdot 40^{0,16} = \qquad (6)$$

$$= 54{,}263102 \div 911{,}71198 \ {}^0C$$

Heat disposed of workpiece is:

$$Q_p = 0{,}885 \cdot (54{,}263102 \div 911{,}71198) \cdot 0{,}0198 \cdot$$

$$\cdot \sqrt{43{,}2 \cdot 470 \cdot 7790 \cdot \frac{\pi \cdot 25{,}15 \cdot 280}{1000} \cdot 0{,}0025} =$$

$$= 2812{,}325341 \div 47251{,}82695 \text{ J} \qquad (7)$$

As a feature those above, the surface specific heat, representing heat transmitted to the part during of the cutting process, reported the contact area and represented by:

$$C_s = \frac{Q_p}{B \cdot L} \qquad (8)$$

will determine changes in the superficial layer of the part structure.

So:

$$C_s = \frac{2812{,}325341 \div 47251{,}82695}{19{,}8 \cdot 2{,}5} = \qquad (9)$$

$$= 56{,}814653 \div 954{,}582362 \text{ J/mm}^2$$

Such due to the effect thermal from area of cutting, abrasive cutting disks are subjected to the action of high temperatures up to 800 - 1000 ^{0}C and pieces, because the same heat effect, supports, in turn, the negative effects of such high temperatures: structural changes, dilation and therefore different added treatment by those considered initially, changes in surface hardness and microhardness, and in borderline cases, where regimes are too intense and the cooling is insufficient, even burns occur on the surface of parts.

Also, by transmission heat into the machine table, if command and control systems are affected by this phenomenon, errors can occur even in the process by active control and geometric control, with negative consequences on the size and shape precision of the parts (for example, advance implementation of the order by retirement due to expansions or changes in machining allowance of supplementary loading technological system elastic of the car).

2. DIMENSIONAL CALCULATION ERROR OF PARTS PROCESSED BY CONTROL WITHOUT THE CORRECTION CENTRE

The factors listed above, which depends the temperature of the workpiece by grinding, producing significant thermal errors, which can be determined from the formula known to change dimension part, with great implications on the accuracy of measurement.

Dimensional error of the part is given by:

$$\Delta d = d \left(\alpha_1 \Delta t_1^0 - \alpha_2 \Delta t_2^0\right) \qquad (10)$$

or:

$$\Delta d = d \left[\alpha_p \left(t_{fp}^0 - t_{0p}^0\right) - \alpha_d \left(t_{fd}^0 - t_{op}^0\right)\right] \qquad (11)$$

where: Δd represents dimension variation part (measurement error) in mm;

d - nominal value of the size measured in mm;

α_p - coefficient of linear expansion of the part to be measured;

t_{op}^0 - initial temperature of the workpiece in degrees Celsius;

t_{fp}^0 - final temperature of the workpiece in degrees Celsius;

When the ambient temperature of measurement devices and work piece are equal with 180C, then the formula (1) becomes:

$$\Delta d = d \ \alpha_p \left(t_{fp}^0 - t_{op}^0\right) \qquad (12)$$

Following the experimental measurements were measured initial and final temperatures, the processing with or without cooling liquid, obtaining the following values:

- t_{op} = 18^{0}C, initial temperature of the part;
- t_{fp} = 266^{0}C, final maximum temperature of the part, worked without coolant.

Linear coefficient of expansion of the part for steel is α_p=13.6·10^{-6} and replacing values in formula (12), the error by measurement results at the same temperature as with size:

$$\Delta d = 25{,}15 \cdot 13{,}6 \cdot 10^{-6} (266 - 18) = 0{,}00848 \text{ mm}$$

Given value is enough high and has a negative influence on the regulation of active control systems of the model Machine and also the

accuracy of processing by an additional dilation of the parts can change the final quota.

3. FINITE ELEMENT ANALYSIS

For a plane problem of temperature at a point in the part, it is based on the location of this point and time:

$$\theta = f\left(x,\ y,\ t\right) \qquad (13)$$

equation representing the field of temperature by which can determine the temperature of each point specified by coordinates x and y and the time where the determined that temperature.

If the temperature do not vary in time the temperature field is stationary. Cases in which considered temperature varies in time, define non-stationary or transient temperature fields. Inside the field there will isothermal surfaces with points with the same temperature.

To analyze flat in two-dimensional fields, points of equal temperature can be found on isothermal curves. Be observed that in the area two-dimensional and stationary the function temperature is similar function movement δ (x, y) in problems of plane elasticity.

For the thermally balance an important parameter is the temperature flow Q [W], which represents quantity of heat that pass in unit time through an isothermal surface and is determined by the relationship:

$$Q = \int_s q\ \mathrm{ds} \qquad (14)$$

where: q - represents intensity flow or unitary heat flow, measured in $\left[W / m^2\right]$.

Intensity heat flow on determined by:

$$q = -\lambda \cdot \nabla\theta \qquad (15)$$

that: λ - is a coefficient of thermal conductivity [W/m·K], which is a characteristic of the material;

∇θ - is called the temperature gradient and represents temperature increase related to the isothermal surface;

θ - temperature of points the surface transmitting heat:

$$grad\ \theta = \lim \left|\frac{\Delta\theta}{\Delta n}\right|_{\Delta n \Rightarrow 0} = \frac{\partial\theta}{\partial n}, \qquad (16)$$

where: $\frac{\partial}{\partial n}$ - is the differential operator which indicates the direction and sense of heat propagation along the normal to in isothermal of decreasing temperature (Figure 4).

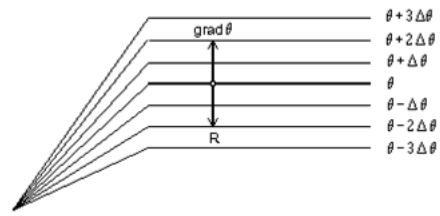

Fig. 4. Meaning and direction of heat propagation.

Variation of temperature in stationary regime is expressed by conduction differential equation or Fourier's equation.

$$\lambda\left(\frac{\partial^2\theta}{\partial x^2} + \frac{\partial^2\theta}{\partial y^2}\right) + M = 0 \qquad (17)$$

in which: M - is flow of internal sources of heat $\left[W / m^3\right]$

This equation describe phenomenon in a general sense, for each particular case is necessary to impose specific conditions for unicity.

Solving problems of thermal requires knowledgel conditions of the outline in order to obtain unique solutions for systems of equations results.

Such, for certain parts may imposed temperature, intensity of heat flow normal to the surface and convective heat exchange (Figure 5) as follows: $Q_{S_1} = f\left(x, y\right)$, S_1 represents the surface of part where the temperature are imposed;

$$q = \lambda\left(\frac{\partial^2\theta}{\partial x^2} n_x + \frac{\partial^2\theta}{\partial y^2} n_y\right),$$

represents surface thermally flow required in S_2, placed by executives cos n_x and n_y;

$\alpha\left(\theta - \theta_E\right)$, means convective heat exchange;

α - is the coefficient of convection at the surface S_3;

θ_E - outside environmental temperature.

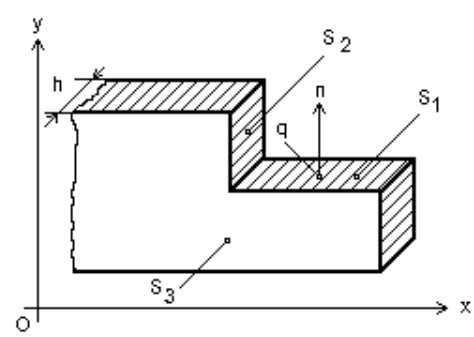

Fig. 5. Convective heat exchange.

To achieve the proposed issue, in the range of subject to processing samples the model without center grinding machine was used to study the transmission of heat in finite element part, a material with following geometry, mechanical and heat: OLC45, L = 19,8 mm; D = 25,15 mm E = $2{,}1\cdot 10^5$ MPa, Young's elasticity module; $\gamma = 0{,}3$ is the coefficient of contraction Poisson; K = 0,0445W/mm^{0}C thermal conductivity; $\alpha=13{,}6\cdot 10^{-6}$ 1/^{0}C coefficient of thermal expansion; b = $0{,}7\cdot 10^{-3}$ convection coefficient (steel - coolant).

Thermal loading was considered the structure of the play, on line of contact with the cutting abrasive disk with temperature T = 900 ^{0}C, and in rest of the knots on the exterior surfaces, with a temperature T = 30 ^{0}C.

As thermal analysis finite element program NISA II, were obtained in each file that shows the temperature of the mesh knot, as shown in Figure 6.

Also, from static analysis, in main uncertainties resultsnamely: movements on the three axes x, y, z of each knot, thus determining module of the thermal expansion movements and the size of structure of part. Such, using the static analysis of part structure by finite element, was performed static analysis due to thermal loads all knots part structure, resulting graphical representations in Figures 7 and 8. Thus, in Figure 7, is presented the variation radius of the part, upon the direction y at 900^{0}C, which affect both the increase as well as processing of the active phase of the process control technology.

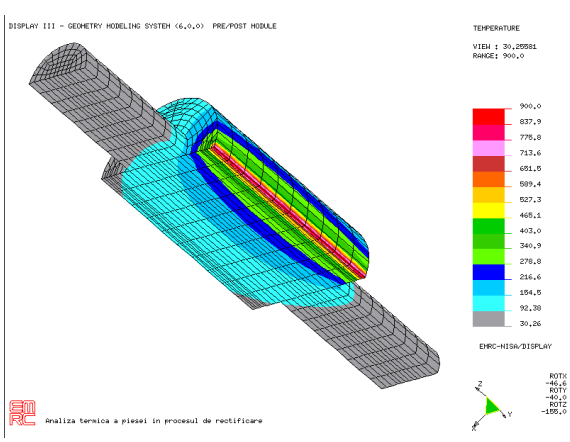

Fig. 6. Temperature variation in part section

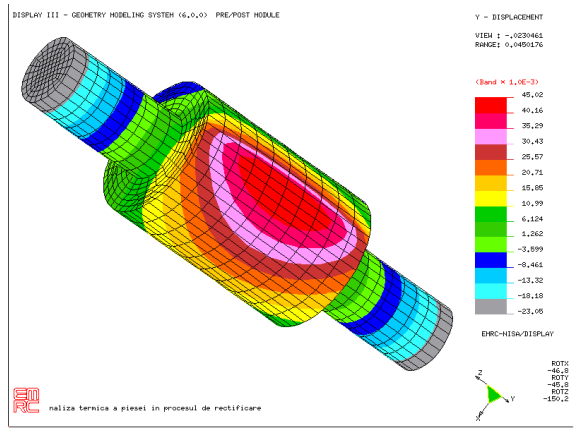

Fig.7. Variation of surface movement at 900^{0}C

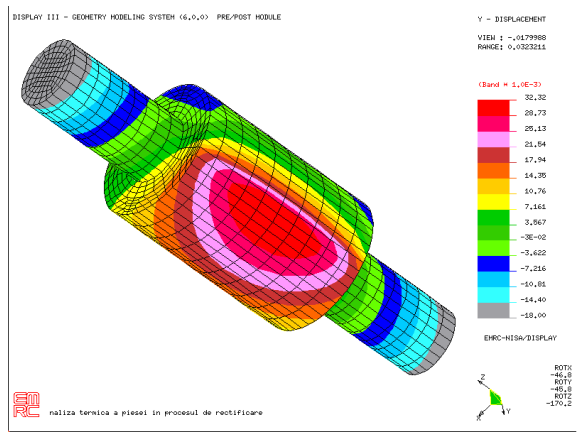

Fig. 8. Variation of surface movement at 800^{0}C

Thermal analysis of part structure are imposed temperature at abrasive disk to contact area with the cutting, focused on determining the variation of temperature and heat flow in the structure of part. For this is used thermal finite element analyze program ANSYS v12, from the mesh structure of part, Figure 9 and setting arc of contact on part generator, Figure 10 for an initial set of data including: environmental diameter of the processed portion to part 25.15 mm, 19.8 mm length segment processed, the generator worked part arc width 2.5 mm, 20^{0}C initial temperature to part, the maximum temperature in the cutting the disk contact area with the maximum processing 900^{0}C and 5 seconds.

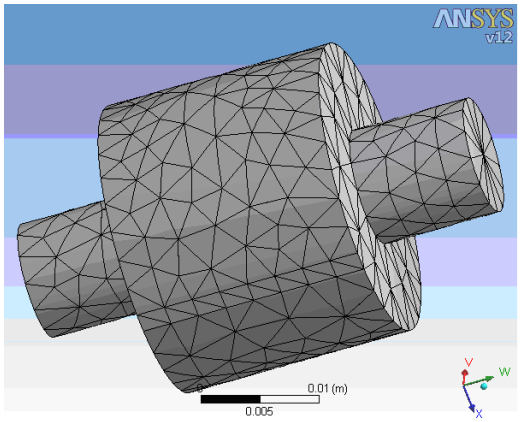

Fig. 9. Finite element meshing to the structure of part

They obtained a number of systematized dates in Table1and Graph of variation of the global temperature minimum starting from the initial temperature of the piece of 16.828^{0}C, to minimum global temperature 266.25^0 C (Figure 11) after close of the processing.

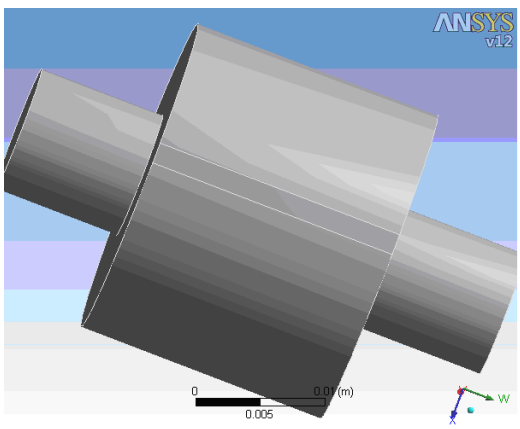

Fig. 10. Contact area of arc between the workpiece and abrasive disk

Tabel I

Changes in global temperatures minimal

Time [s]	Minimum [°C]	Maximum [°C]
5.e-002	18.137	900.
8.0846e-002	17.517	
0.10725	16.828	
0.13366	17.56	
0.19674	20.002	
0.29388	20.017	
0.44291	20.167	
0.67304	21.259	
1.0311	26.834	
1.5311	43.527	
2.0311	67.976	
2.5311	98.024	
3.0311	131.44	
3.5311	166.38	
4.0311	201.41	
4.5311	235.55	
5.	266.25	

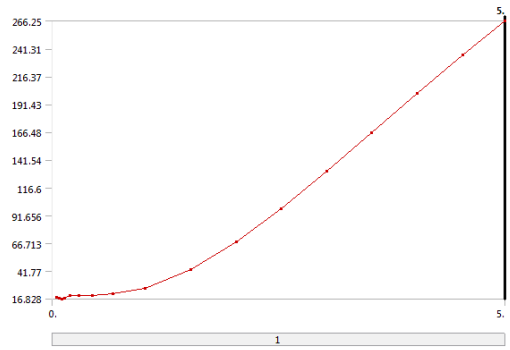

Fig. 11. Changes in global temperatures minimal

Temperature variation of workpiece surface from maximum value of the processing area to the minimum value is shown in figure 12 and three-dimensional representation in Figure 13.

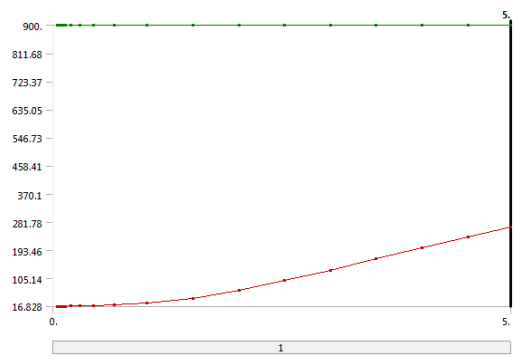

Fig. 12. Changes in global temperature maximum

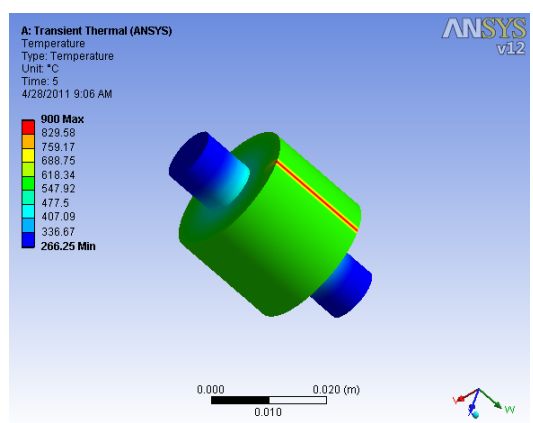

Fig. 13. Temperature variation on workpiece surface

The dates systematized in Table 2 and Figure 14 represents the variation of heat flux on the surface directional part.

Tabel 2
Variation of directional heat flow

Time [s]	Minimum [W/m²]	Maximum [W/m²]
5.e-002	-3.3962e+007	4.5057e+007
8.0846e-002	-2.0754e+007	3.6283e+007
0.10725	-1.6549e+007	3.2229e+007
0.13366	-1.4185e+007	2.9626e+007
0.19674	-1.1071e+007	2.6274e+007
0.29388	-8.5136e+006	2.3528e+007
0.44291	-6.4638e+006	2.1322e+007
0.67304	-4.8711e+006	1.9563e+007
1.0311	-5.4712e+006	1.8166e+007
1.5311	-6.4476e+006	1.7128e+007
2.0311	-7.0563e+006	1.6488e+007
2.5311	-7.4708e+006	1.6055e+007
3.0311	-7.7689e+006	1.5744e+007
3.5311	-7.9906e+006	1.5512e+007
4.0311	-8.1597e+006	1.5335e+007
4.5311	-8.2908e+006	1.5197e+007
5.	-8.3891e+006	1.5093e+007

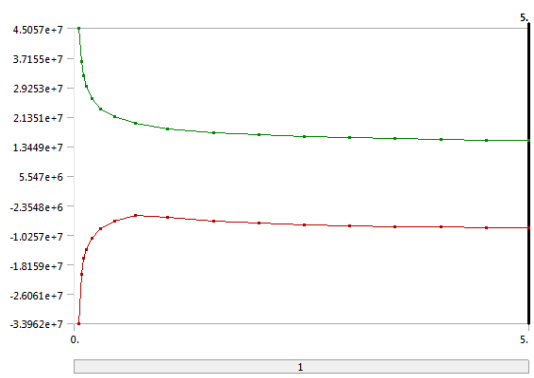

Fig.14 . Directional heat flow variation

The dates systematized in Table 3 and Figure 15 represents the total heat flux variation on the workpiece surface.

Tabel 3
Variation of total heat flow

Time [s]	Minimum [W/m²]	Maximum [W/m²]
5.e-002	0.51781	5.3041e+007
8.0846e-002	0.59279	4.6252e+007
0.10725	1.2643	4.3259e+007
0.13366	2.1707	4.1404e+007
0.19674	7.1618	3.9121e+007
0.29388	31.693	3.7365e+007
0.44291	122.46	3.6043e+007
0.67304	329.21	3.5054e+007
1.0311	564.16	3.4314e+007
1.5311	615.38	3.3792e+007
2.0311	524.68	3.3483e+007
2.5311	434.01	3.3279e+007
3.0311	418.99	3.3135e+007
3.5311	302.49	3.303e+007
4.0311	246.97	3.2951e+007
4.5311	443.12	3.2889e+007
5.	500.82	3.2843e+007

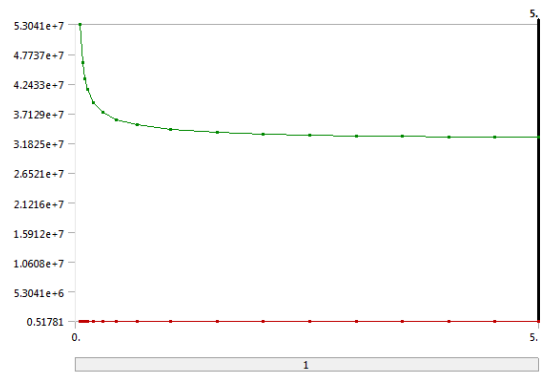

Fig. 15. Variation of total heat flow

Under the action of high temperature in cutting zone, on arc of contact between the cutting abrasive disc and workpiece occurs variation to heat flow, transmitted in its entire mass.

Variation of the total and directional heat flow during the 5 seconds of processing is systematized in Table 4, and three-dimensional representation to total and dimensional heat flow is observed in Figures 16 and 17.

Tabel 4
Variation of heat flow during processing

Value	*Temperature*	*Total heat flow*	*Direcţional heat flow*
Rezultate			
Minim	266.25 °C	500.82 W/m²	-8.3891e+006 W/m²
Maxim	900. °C	3.2843e+007 W/m²	1.5093e+007 W/m²
Valoarea minimă pe parcursul prelucrării			
Minim	16.828 °C	0.51781 W/m²	-3.3962e+007 W/m²
Maxim	266.25 °C	615.38 W/m²	-4.8711e+006 W/m²
Valoarea maximă pe parcursul prelucrării			
Minim	900. °C	3.2843e+007 W/m²	1.5093e+007 W/m²
Maxim	900. °C	5.3041e+007 W/m²	4.5057e+007 W/m²

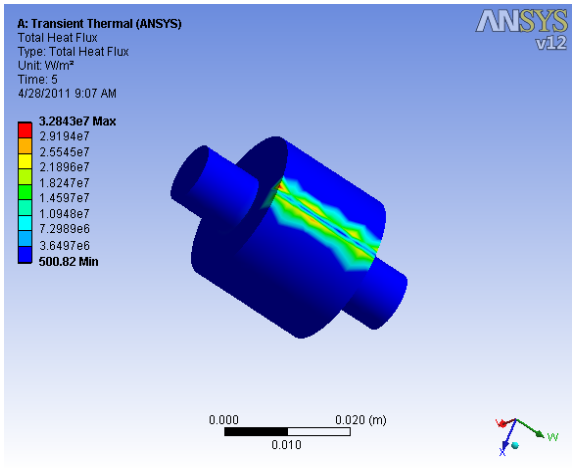

Fig. 16. Variation of total heat flow

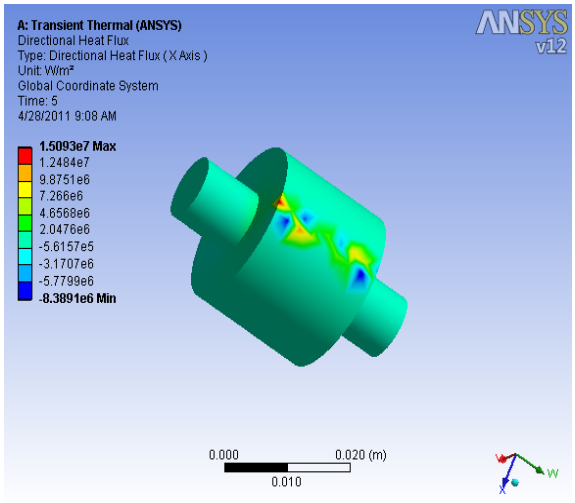

Fig. 17. Variation of heat flow in the direction x

Maintain constant temperature in the area and therefore and whole structure to centerless grinding in order to maintain constant cutting regime parameters can be successfully achieved by controlling the working cycle by using computer assisted adaptive control, which is equipped the machine with cross feed. As this control method was used of the processing cycle technology, which instead of using transverse advance continuous adjusted by the machine systems was used by processing pressure on to feed disk and adjustable constant throughout the processing.

4. CONCLUSIONS

Following the experimental measurements and theoretical analysis by the classical method using modern analytical and finite element can draw some conclusions, as follows:

- due to the emergence of such high temperatures in the processing area, there were significant strain due to expansion of the parts processed by grinding centerless with cross feed;
- was observed, as expected, that when using liquid cooling, obviously decrease the effects of temperature increase in area disposed of part of the cutting, which diminishes the possibility of expansions and establishment of the position of working parts in the machine grinding centerless with cross feed;
- maintaining constant temperature in the area and thus in entire structure of to grinding machine centers in order to maintain constant cutting regime parameters can be successfully achieved by using active control and cycle control with the computer work electronically model fitted to the grinding machine centers which experiments were conducted;
- using the finite element method to obtain theoretical dates approaching that magnitude and value of those obtained by experiment, so this method can be successfully used to analyze temperature influence on the process of machining to parts.

REFERENCES

[1] Cernăianu, A.C., *Contribuţii privind controlul automat al parametrilor tehnologici de proces la prelucrarea prin rectificare fără centre*, Teză de doctorat, Universitatea din Craiova, 1997.

[2] Cernainau, A.C., *Maşini-Unelte. Elemente de proiectare. Organologie şi cinematică*, Editura Universitaria, ISBN 973-742-024-1, Craiova, 540 pag. 2005.

[3] Hărădău, M., Metoda elementelor finite, P-Transilvania Pres, Cluj-Napoca, 1995.

[4] Maslov, H.E., Teoriia şlofovaniia materialov, Moskva, Maşinostroienie, 1974.

[5] Oprean, A., Sandu, I. Gh., Minciu, C. ş.a., Bazele aşchierii şi generării suprafeţelor, Editura Didactică şi Pedagogică, Bucureşti, 1981.

[6] Şteţiu, G, Lăzărescu, I., Oprean, C., Şteţiu, M., Teoria şi practica sculelor aşchietoare, vol. 1. Elemente de teoria aşchierii metalelor, Editura Universităţii din Sibiu, Sibiu, 1994.

ON SAME THERMODYNAMIC PROPRIETES OF LIQUEFIED METHANE AND THERMODYNAMIC PROCESSES INVOLVED IN THE TRANSPORT AND STORAGE OF LIQUEFIED NATURAL GAS

Tudora CRISTESCU

OIL-GAS UNIVERSITY PLOIEŞTI, Romania

Rezumat*:* Lucrarea conţine date şi relaţii de calcul privind unele proprietăţi termodinamice ale metanului lichid. De asemenea sunt prezentate exemple numerice în cazul unor procese termodinamice posibil implicate în fluxul tehnologic al gazului natural lichefiat.
Cuvinte cheie: metan lichid; proprietăţi termodinamice; procese termodinamice.

Abstract: Data and formulae for thermodynamic properties of liquefied methane are presented. Additionally, numerical examples are presented for some thermodynamic processes putatively involved in the natural liquefied gas technological flux.
Keywords: liquid methane; thermodynamic properties; thermodynamic processes.

1. INTRODUCTION

Liquefaction of natural gases is employed when they cannot be transported via pipelines. LNG (liquefied natural gas) actually stands for liquefied methane; it can be considered as complementary energy source. The technological flux of exploitation of LNG involves the following steps: Natural gas extraction (gaseous state) Natural gas transport via pipelines Natural gas liquefaction (resulting in liquid methane) Sea transportation of liquid methane Liquefied methane storage Liquefied methane vaporization (resulting in gaseous methane) followed by heating of the gaseous methane Storage/Transport/Delivery of gaseous methane Consumer. These steps involve a series of thermodynamic processes. Among the processes possibly involved are: thermodynamic transformations (isobar heating or cooling), iso-enthalpy expansion, iso-entropy compression or expansion, phase transitions (liquefaction, vaporization), heat transfer. This means that not only gaseous but also liquid methane are both increasingly important as thermodynamic agents. Thus, we take an opportunity to present some thermodynamic aspects involving liquefied methane. Methane is a pollutant since its combustion results in greenhouse gases. The storage, transport and use of LNG involve (more so than for other fuels) special standards of operation regarding maintenance, feasibility, safety, fire prevention and extinguishing. Liquid methane is a cryogenic fluid i.e. it is a substance used in cooling cycles for extremely low temperatures, or for its own liquefaction. Per ISCIR technical standards, liquefied methane and LNG are classified in group C (strongly cooled liquefied gases), methane in category 7b, and natural gas in category 8b, as mixtures of flammable gases.

2. THERMODYNAMIC PROPERTIES OF LIQUEFIED METHANE

Methane thermodynamic parameters:
Chemical formula: (CH_4); Molar mass: M = 16.04 kg/kmol; Gas constant: R = 518.722 J/(kg K); Self-ignition temperature: t_a = 537 ^{0}C; Theoretical combustion temperature: t_t =2040°C; Lower caloric power: H_i = 49949 kJ/kg; H_i = 35797 kJ/m^3_N; Limits for air-mixture explosion: 5...15%.

At temperature 0^0 C and pressure p =760 torr: Density ρ = 0.7168 kg/m^3; Mass caloric capacity, c_p = 2.117 kJ/(kg K). At pressure p =760 torr: Specific latent melting heat: r_t = 58.615 kJ/kg; Melting temperature: t_t =-182.5 ^{0} C (T_t =90.65 K);

Specific latent vaporization heat: r_v = 548.471 kJ/kg; Vaporization temperature: t_v =-161.7 ^{0}C (T_v =111.45 K). Liquid phase temperature at vaporization temperature: ρ_v = 415 kg/m^3;

Methane parameters at critical point: Critical temperature: t_{cr} = - 82.5 ^{0}C (T_{cr} = 190.65 K); Critical pressure: p_{cr} = 46.29 bar; Critical density: ρ_{cr} = 161.8 kg/m^3; Compressibility factor at the critical point: Z_{cr}=0.289;
Acentric factor: ω=0.0104.
Triple State Properties: Temperature: t_{tr} = - 182.45 ^{0}C (T_{tr} = 90.7 K); Pressure: p_{tr} = 11.7 kPa;
The van der Waals constants for methane are: a = 535.434 Nm^4/kg^2; b = 2.058 dm^3/kg.
The following formulae are proposed in the literature for evaluation of some thermodynamic properties of methane.
Density [kg/m^3]:

$$\rho = 183.9285 + \sqrt{-60932.1 - 744.0476 \cdot t} \qquad (1)$$

in the temperature range -180…- 85 ^{0}C, with temperature expressed in ^{0}C in (1).

Viscosity [cP]:

$$\log\mu = -11.67 + \frac{499.3}{T} + 8.125 \cdot 10^{-2} \cdot T - \\ - 226.3 \cdot 10^{-6} \cdot T^2 \qquad (2)$$

in the temperature interval -180…- 80 ^{0}C.
Mass caloric capacity [J/(kg K)]:

$$c = -79.7212 \cdot 10^2 + 290.223 \cdot T - \\ - 246.676 \cdot 10^{-2} \cdot T^2 + 705.31 \cdot 10^{-5} \cdot T^3 \qquad (3)$$

in the temperature range 93…181 K.
Thermal conductivity [W/mK]:

$$\lambda = 0.635914 - 57.4998 \cdot 10^{-4} \cdot T + \\ + 156.975 \cdot 10^{-7} \cdot T^2 \qquad (4)$$

in the temperature range 73…173 K, with temperature (2)-(4) expressed in Kelvin.
Superficial tension [N/m]:

$$\sigma \cdot 10^3 = -12.339723 - 151.83007 \cdot 10^{-3} t - \\ - 129.13783 \cdot 10^{-6} \cdot t^2 - 1233.6036 \cdot 10^{-9} t^3 \qquad (5)$$

in the temperature range -180…-80 ^{0}C, with temperature expressed in ^{0}C in (5).

3. THERMODYNAMIC PROCESSES PUTATIVELY INVOLVED IN NATURAL LIQUEFIED GASES TRANSPORT AND STORAGE

a) Joule-Thomson effect for a van der Waals gas

Pressure decreases in an iso-enthalpy expansion. The thermal effect of iso-enthalpy expansion was experimentally shown by James Prescot Joule and its theory studied by William Thomson (lord Kelvin). The Joule-Thomson effect expresses the variation of temperature with pressure when enthalpy is constant. The Joule–Thomson effect for real gases results in either temperature increase or decrease. The *Joule – Thomson coefficient*, μ_{J-T} is defined as:

$$\mu_{\text{J-T}} = \left(\frac{\partial T}{\partial p}\right)_h \qquad (6)$$

The initiation of a thermal effect when a gas passes a narrowing section from a high pressure area to a lower pressure area only takes place if the gas has a behavior different from a perfect gas. For a finite pressure variation, the temperature variation is computed as:

$$(\Delta T)_h = (T_2 - T_1)_h = \int_{p_1}^{p_2} \frac{T\left(\frac{\partial v}{\partial T}\right)_p - v}{c_p} \mathrm{d}p \qquad (7)$$

which is the *integral Joule – Thomson effect*. For real gases the Joule–Thomson effect results in a temperature increase or decrease as a function of the numerator of (7). In iso-enthalpy expansion pressure always decreases, which results in one of the following situations:
- temperature decrease:

$$\left(\frac{\partial v}{\partial T}\right)_p > \frac{v}{T}, \text{ thus } \left(\frac{\partial T}{\partial p}\right)_h > 0 \text{ and } \mu_{J-T} > 0 \qquad (8)$$

- temperature increase:

$$\left(\frac{\partial v}{\partial T}\right)_p < \frac{v}{T}, \text{ thus } \left(\frac{\partial T}{\partial p}\right)_h < 0 \text{ and } \mu_{J-T} < 0 \qquad (9)$$

- temperature remains constant:

$\left(\frac{\partial v}{\partial T}\right)_p = \frac{v}{T}$, thus $\left(\frac{\partial T}{\partial p}\right)_h = 0$

and $\mu_{J-T} = 0$ (10)

For van der Waals gases, the temperature change in an iso-enthalpy expansion, when pressure decreases from p_1 to p_2, is computed as:

$$(T_1 - T_2)_h \Big|_{p1}^{p2} = T_1 - \\ -\sqrt[3]{T_1^3 - 3\mathrm{a}(p_1 - p_2) + \frac{3\mathrm{b}}{2}\left(p_1^2 - p_2^2\right)} \quad (11)$$

where a and b are the van der Waals constants specific for the considered gas.

b) Vaporization/liquefaction

LNG vaporization is the transformation from liquid to gas of methane at vaporization temperature t_v and pressure p_v; liquefaction is the reverse of vaporization. The two processes are isobar and isothermal when neglecting pressure losses. During vaporization/liquefaction the system (in this case, methane) receives/loses heat from/to the exterior. The received/lost heat by m =1 kg methane to change to gas/liquid state is computed as:

$$q_v = h^{II} - h^{I} = r \quad (12)$$

c) Heating/cooling

Heating/cooling of LNG is isobar (assuming negligible pressure losses). During heating/cooling, the system (in this case, methane) receives/loses heat from/to the environment. The received/lost heat of m =1 kg of liquid methane for isobar change from State 1 to State 2 is computed as follows:

$$q_{12inc/racire} = h_2 - h_1 \quad (13)$$

or

$$q_{12,inc/racire} = c_p(t_2 - t_1) \quad (14)$$

d) Isothermal expansion

Second thermodynamic principle states:

$$\delta q = T\mathrm{d}s \quad (15)$$

The heat exchanged in an isothermal reversible transformation is expressed as:

$$q_{12T} = T\int_{p_1}^{p_2}\left(\frac{\partial s}{\partial p}\right)_T \mathrm{d}p = -T\int_{p_1}^{p_2}\left(\frac{\partial v}{\partial T}\right)_p \mathrm{d}p \quad (16)$$

The partial derivative $\left(\frac{\partial v}{\partial T}\right)_p$ is computed using the gas state equation. For a perfect gas, by using the state specific equation in an isothermal expansion from pressure p_1 to pressure p_2, we obtain:

$$q_{12T} = \mathrm{R}T\ln\frac{p_1}{p_2} \quad (17)$$

Isothermal expansion of gases is used in cryogenic applications, in order to maintain liquefied masses at constant temperature in storage during transportation. Consider a liquefied gas under thermodynamic saturation. Then the heat exchanged by 1 kg of substance to change aggregation state from liquid to gas is r_v (latent specific vaporization heat). Denote by q_S [W/m^2] a unitary thermal flux received by a system per1 m^2 and time unit. From the energy balance equation:

$$\dot{m}_S\, r_v = q_S \quad (18)$$

we can compute, $\dot{m}_S$ [kg/(m^{2}s)], the flux liquefied gas for the heat receiving surface unit; $\dot{m}_S$ vaporizes and needs to be evacuated from the storage space:

$$\dot{m}_S = \frac{q_S}{r_v} \quad (19)$$

This method for maintaining constant temperature is simple and easy to implement. The evacuated gas is used for powering thermal engines of maritime transportation ships, supplied to consumers, or stored.

4. CASE STUDIES

a) Volume decreasing by liquefaction

Natural gas liquefaction has as main advantage the significant volume reduction of gas. The volume occupied by 1 kg of liquid methane, at pressure p = 1 atm and temperature t_v = -161,7 ^{0}C is 579 times smaller than the volume occupied by the same methane quantity in gaseous state at p = 1 atm and t = 0 ^{0}C.

b) Evaluation of some thermodynamic properties of liquefied methane

Table 1 contains the results of the evaluation of some thermodynamic properties of liquid methane, using (1)...(5).

c) Evaluation of the Joule-Thomson effect for methane, assuming van der Waals model

Table 2 contains the results of the evaluation of temperature decrease during iso-enthalpy expansion of methane, by using (11). The computation assumes the simplification that methane obeys a van der Waals state equation.

c) Vaporization of liquid methane (obtaining gaseous methane) and heating of gaseous methane

The received heat by m =1 kg methane to change to gas state, if p = 1 atm and t_v = -161,7 ^{0}C, using (12), is $q_v = 548$ kJ/kg. The received heat by m =1 kg de methane, using (14) for isobar heating to t = 20 ^{0}C is $q_{12inc} = 380$ kJ/kg.

Results: $q_{v+12inc} = 928$ kJ/kg.

d) Isothermal expansion

Constant temperature of liquefied gas is maintained by an isobar-isothermal process where the heat received by the liquefied gas (by thermal exchange with the environment) is used for the vaporization of some part of the liquid mass. The liquefied gas is at thermodynamic saturation, thus the heat exchanged by a 1 kg of substance is r_v - the vaporization latent specific heat; table 3 contains values for this thermodynamic property. Consider a unit thermal flux corresponding to the addition of q_S =100 W/m^2 heat to the 1 m^2 surface during the unit of time. We use (19) for evaluating the liquefied gas flux q_S =100 W/m^2 corresponding to the unit of surface, which vaporizes and needs to be evacuated from the storage space. Table 3 contains values for the liquefied gas mass corresponding to the unit of surface.

5. CONCLUSIONS

- Romania can use LNG as complementary source of energy, as fuel for heat producing combustion.
- LNG is a high purity fuel, which contains only methane.
- Methane is a polluting fuel, since its combustion results in greenhouse gases.
- Through liquefaction the gas volume decreases substantially (~600 times) which facilitates long distance transportation.
- Liquefaction, transportation, storage, re-liquefaction and vaporization of LNG involve a vast variety of thermal process.
- Iso-enthalpy expansion is an irreversible thermodynamic transformation where enthalpy is maintained constant and is accompanied by certain thermal effects (increasing or decreasing of temperature) and needs to be accounted for in the industrial exploitation and transportation of hydrocarbons. For methane, under a van der Waals assumption, lamination results in a temperature decrease of about 0.1…1.4 K.
- When heat is added from the environment to the stored fluid, the simplest method to maintain constant temperature is isothermal expansion which results in the evacuation of some liquid mass, which vaporizes by intake of the added heat. The method is simple and easy to implement; the evacuated gas is used for powering thermal engines of maritime transportation ships, supplied to consumers, or stored. The LNG quantity that vaporizes and needs evacuation depends on the stored fluid type, the storage temperature and pressure, and the storage conditions.
- The data we presented on liquid methane properties may constitute the bases for elaborating complex computational programs.
- Vaporization of large quantities of LNG results in large cold quantities, with an important polluting effect.

Table 1
Thermodynamic properties of liquefied methane

Thermodynamic properties	Temperature T, [K]	Temperature t, ^{0}C	Value
Density, ρ, [kg/m^3]	93.15	-180	454.107
	103.15	-170	439.967
	113.15	-160	425.00
	123.15	-150	409.04
	133.15	-140	391.858
	143.15	-130	373.122
	153.15	-120	352.314
	163.15	-110	328.542
	173.15	-100	300.000
	183.15	-90	261.596
Viscosity, μ, [cP]	100	-173.15	9.185
	110	-163.15	0.117
	120	-153.15	0.096
	130	-143.15	0.081
	140	-133.15	0.068
	150	-123.15	0.057
	160	-113.15	0.045
	170	-103.15	0.035
	180	-93.15	0.025
	190	-83.15	0.017
Caloric mass capacity at constant pressure, c_p, [J/(kg K)]	100	-173.15	3435.68
	110	-163.15	3492.29
	120	-153.15	3521.05
	130	-143.15	3564.29
	140	-133.15	3664.31
	150	-123.15	3863.44
	160	-113.15	4204.00
	170	-103.15	4728.31
	180	-93.15	5478.67
Thermal conductivity, λ [W/(mK)]	80	-193.15	0.2763796
	90	-183.15	0.2455655
	100	-173.15	0.2178910
	110	-163.15	0.1933559
	120	-153.15	0.1719604
	130	-143.15	0.1537043
	140	-133.15	0.1385878
	150	-123.15	0.1266107
	160	-113.15	0.1177732
	170	-103.15	0.1120751
Superficial tension, $\sigma \bullet 10^3$, [N/m]	93.15	-180	17.99999
	133.15	-140	9.770393
	173.15	-100	2.78581

Table 2
The integral Joule – Thomson effect for methane

Initial temperature, t_1, [^{0}C]	Initial temperature, T_1, [K]	Initial pressure, p_1, [bar]	Final pressure, p_2, [bar]	Temperature variation, ΔT, [K]
-153.15	120	1.9	1	0.1
-100	173.15	30	1	1.4
-120	153.15	10	1	0,973

Table 3
Liquefied gas mass flux corresponding to the unit of surface, which vaporizes and needs to be evacuated from the storage space

Storage temperature T, [K]	Abs. Pressure, p, [MPa]	Specific latent vaporization heat, r, [kJ/kg]	Mass flux corresponding to the unit of surface for q =100 W/m^2 $\dot{m}_S \cdot 10^3$, [kg/(m^{2}s)]
100	0.03441	529.8	0.18875
110	0.08820	513.3	0.19482
120	0.19158	494.2	0.20234
130	0.36760	471.7	0.21200
140	0.64165	444.8	0.22482
150	1.04065	412.3	0.24254
160	1.59296	372.0	0.26882
170	2.32936	320.0	0.31250
180	3.28655	246.2	0.40617
190	4.52082	79.8	1.25313

Notations

c - Mass caloric capacity, J/(kg K)
H – Caloric power, J/kg; J/m^3_N
h - Mass enthalpy, J/kg
q - Mass heat, J/kg
$\dot{Q}$ - Thermal flux, W
$\dot{m}$ - Thermal mass debit, kg/s
M – Molar mass, kg/kmol
p – Pressure, Pa, bar
r - Phase transition specific latent heat, J/kg
R – Gas constant, J/(kg K);
t – Temperature (^{o}C)
T - Temperature (K)
Z – Compressibility factor
λ - Thermal conductivity W/(mK):
μ - Dynamic viscosity, cP:
ρ – Density, kg/m^3
σ - Superficial tension, N/m,
ω - Acentric factor

Subscript

a - self ignition
abs - absolute
consum - at consumer
cr - critic
i- inferior
inc - heating
I - saturated liquid
II - dry saturated vapors
J-T - Joule-Thomson
p – constant pressure
primit - needed for heating and vaporization
răcire - cooling
S – per unit surface
t - theoretical
t – melting
tr - triple
T - at constant temperature
v - vaporization

REFERENCES

[1] Cristescu, T., *Thermal properties of hydrocarbon deposits*, Editura Universal Cartfil, Ploieşti, 1998.
[2] Cristescu, T., *Termotehnica*, Editura Universităţii din Ploieşti, 2009.
[3] Cristescu T., Stoicescu M., Stoianovici D., *Liquefied petroleum gases utilization: an assessment,* Buletinul Universităţii Petrol – Gaze din Ploieşti, Seria Tehnică, Vol. LX, No. 4A, Ploieşti, 2008.
[4] Cristescu T., Stoicescu M., Stoianovici D., *On the Utilization of Liquefied Natural Gases*, Proceedings of The Internationally Attended National Conference on Technical Thermodynamics, Conferinţa naţională de termotehnică, cu participare internaţională, (CNT 17), Ediţia a XVII-a, Braşov, 2009.
[5] Cristescu T., Ciobanu, P., *On a Class of Thermodynamic Processes Involved in the Transport and Storage of Liquefied Petroleum Gas*, Buletinul Universităţii Petrol – Gaze din Ploieşti, Seria Tehnică, Vol. LXII, No. 3B, Ploieşti, 2010.
[6] Hera, D., *Technical Cryogenics,* Editura Matrix Rom, Bucureşti, 2002.
[7] Jones, J., B., Dugan, *R., E., Engineering Thermodynamics*, Prentice Hall, Englewood Cliffs, New Jersey, 1996.

[8] Olteanu,B., Stirimin, Şt., Valter, P., Zgîia, I., *Gaseous and liquefied hydrocarbons*, Editura Tehnică, Bucureşti, 1994.
[9] Raznjevic, K., *Thermodynamic tables and diagrams,* Editura Tehnică, Bucureşti, 1978
[10] Şomoghi, V., Pătraşcu, M., Dobrinescu, D., Ioan, V., *Physical properties used in thermal and fluid dynamics,* Universitatea Petrol – Gaze, Ploieşti, 1997.
[11] Winterbone, D., E., *Advanced Thermodynamics for engineers*, Butterworth Heinemann, Oxford, 1997.
[12] Wylen, G., Sonntag, R., Borgnakke, C., *Fundamentals of classical thermodynamics*, John Wiley and Sons, Inc., New York, 1994.
[13] *** C27-85, *Technical recommendations for reservoirs for compressed, liquefied or dissolved.*

ASPECTS CONCERNANT L'UTILISATION DES ÉQUIPEMENTS MOBILES DE COMPACTAGE DES DÉCHETS TYPE SCIURE

Petre RĂDUCANU[1], Carmen PAPADOPOL[1], Veneţia SANDU[2], Romain FERNIQUE[3]

[1]UNIVERSITE POLYTECHNIQUE DE BUCAREST, Roumanie;
[2]UNIVERSITE TRANSILVANIA BRASOV, Roumanie;
[3]UNIVERSITE DE TECHNOLOGIE DE BELFORT-MONTBELIART, France

Rezumat. Exploatarea importantului fond forestier al României conduce şi la obţinerea unor mari cantităţi de deşeuri, printre care şi rumeguşul, deşeuri care, dacă nu sunt tratate cu grijă, pot produce o intensă poluare şi o risipă inadmisibilă. O metodă eficientă de eliminare a acestor neajunsuri se poate realiza prin uscarea şi compactarea acestor produse secundare sub formă de brichete, care pot fi valorificate prin ardere în diverse instalaţii termice. Reglementările cuprinse în legislaţia UE în domeniul ecologic şi anume de a se valorifica integral deşeurile lemnoase rezultate în urma prelucrărilor primare şi secundare se respectă prin plasarea unor echipamente de compactare staţionare înserate în fluxul tehnologic specific la fiecare agent economic din domeniu. O soluţie superioară o reprezintă utilizarea unui echipament mobil, care poate fi deplasat la diverşi utilizatori.
Cuvinte cheie: deşeuri, brichete, flux tehnologic.

Abstract. L'exploitation de l'importante réserve forestière de la Roumanie conduit aussi à l'obtention de grandes quantités de déchets, parmi lesquels la sciure aussi, des déchets qui traités négligemment peuvent produire une intense pollution et un gaspillage inadmissible. Une méthode efficiente pour éliminer ces désagréments serait le sèchement et le compactage de ces produits secondaires sous forme de briquettes pouvant être valorisées par combustion dans diverses installations thermiques. Les réglementations de la législation UE dans le domaine écologique, plus précisément celles concernant la valorisation intégrale des déchets en bois, résultat des traitements primaires et secondaires, sont respectées par l'emplacement de certaine équipements de compactage stationnaire, insérés dans le flux technologique spécifique pour chaque agent économique du domaine. Une solution supérieure est l'utilisation d'un équipement mobile, qu'on peut déplacer à certains utilisateurs.
Keywords: déchets, briquettes, flux technologique.

1. PROLOGUE

La Roumanie dispose d'une superficie de forêts d'environ 27% de lq superficie totale du pays. Le fond forestier de la Roumanie est de 0,30 ha/habitant: Ce fond forestier est caractérisé par un repartissement non-uniforme. La plupart des forêts (61%) se trouvent à la montagne, à plus de 700 m d'altitude, 29% sont situées dans la région de collines et seulment 10% des forêts sont situées à la campagne, à une altitude de 150 m où moins.

L'exploitation de cett importante réserve forestière conduit aussi à l'obtention de grandes quantités de déchets qui traités négligemment peuvent produire une intense pollution et un gaspillage inadmissible:

Dans le tableau 1 on présente la composition dimensionnelle des sortiments dans la catégorie déchets (les éclats de bois résultat du nettoyage des sciages pour la cellulose, sciure, bois en éclisse etc).

On remarque que la sciure résultant des coupes dans la forêts d'abitude n'est pas traitée de manière convenable; étant transportée par les eaux de surface dans les ruisseaux et les rivières; avec des conséquences nuisibles pour la faune et la fleure, tenant compte de leur décomposition et de l'effet produit par les substances tannantes résultantés.

Sur 11.000.000 m^3/an de bois massif, 5.000.000 m^3/an sont destinés à l'industrialisation et le reste de 6.000.000 m^3/an sont affectés à la Régie Nationale des Forêts, aux construction de mines et privées. Dans le secteur de l'industrialisationdu bois, on estime une moyenne de 11% de sciure (12% pour les résineux et 10% pour les feuillus).

Résultent ainsi 550.000 m^3/an de sciure.

Tableau 1.
Composition dimensionnelle des sortiments de catégorie déchets

Dimensions des particules componentes [mm]	Structure dimensionnelle pour		
	Éclat de bois [%]	Sciure [%]	Bois en éclise [%]
Sous 0,5	0,5…2,0	5,0…20,0	0,5…6,0
0,5…1,0	1,0…5,0	10,0…30,0	2,0…8,0
au dessus de1,0…3,0	5,0…20,0	60,0…80,0	30,0…50,0
au dessus de 3,0…6,0	10,0…30,0	2,0…20,0	25,0…50,0
au dessus de 6,0…30,0	60,0…80,0	0,0…1,0	20,0…60,0

Dans le secteur de la Régie Nationale des Forêts, le sciage, mines etc on estime 3% de sciure, donc 180.000 m^3/an (correspondant aux 6.000.000 m^3/an de bois massif).

Un autre aspect dont il faut tenir compte est l'utilisation du terrain dans des buts énergétique, chauffage et preparation de la nouriture qui n'ont cessé ni aujourd'hui, raison pour laquelle l'analyse de cet état de fait représante le point de départ pour la conception de nouveaux programmes de dévelopement, au niveau régional et mondial. L'utilisation énergetique du bois a un caractère dispersé et descentralisé; fait pour lequel la qualité aussi des infor,ations statistiques sur les énergies provenant du bois est inférieure à celle provenant des branches industrielles, surtout dans les conditions où cette énergie est consommée directement par les propriétaires de forêtsou par l'industrie forestiére qui ne paient rien pour l'obtenir et qui ne sont pqs obligés de tenir une évidence dans ce but.

Les principaux utilisateurs d'énergie provenant du bois sont les familles (surtout à la campagne); d'abord pour le chauffage propre, l'industrtrie forestière pour couvrir le nécessaire de briquettes, les consumateurs inter,édiaire (les fabricants de briquettes, les fabriquants de ,anganèse, installations locales d'énergie etc):

Par cette analyse, les déchets resultés de l'exploitation du bois peuvent être transfor,és par séchment et co,pactage. Donc, la projection des installations de séch,ent et de co,pactage de déchets en bois s'impose.

2. ANALYSE DES SOLUTIONS CONSTRUCTIVES

Les réglé,entations dans la législation UE dans le do,aine écologique et plus précisément de valorifier intégralement les déchets de bois résultés des traitements pri,aires et secondaires sont respectées, en général, par l'emplacement d'équipements de compactage stationnaires insérés dans le flux technologique spécifique pour chaque agebt économique dans le domaine:

Une analyse technico-économique des possibilités typologiques pour solutionner le séchement et le compactage mène au variantes suivantes:

1. Équipements stationnaires, emplacés dans chaque unité fabricante de matériel en bois.
2. Centres zonales doués d'équipements stationnaires destinés aux unités rapprochées fabricantes de matériel en bois.

Équipements mobiles, de dimensions réduites, déplaçable dans chaque unité de fabrication.

Les équipements stationnaires de séchement et compactage ont quelques désavantages mageurs:

- Grands coûts d'investissement, dûs à la complexité constructive spécifique, donc, ils sont pratiquement inaccessibles pour un utilisateur du type IMM.
- Grandes dimensions, donc occupation permanente d'un espace productif important.
- Impossibilité d'assurer en permanence la matière première, à cause de la fluctuation des quantités de déchets de bois résultant de l'activité propre.
- Activité saisonnière spécifique au domaine, donc manque d'activité de l'équipement pour longtemps.

La deuxième vqriqnte, celle de centres zonales de briquetage des déchets en bois n'est pas justifiée dans notre pays pour les raisons suivantes:

- Dispersion des traiteurs de bois, qui d'abitude sont emplacés à la montagne.
- Le manque d'efficience du transport en respectant les règles de la protection de l'environnement.
- La difficulté de déter,iner la capacité du centre zonale par raport aux productions variables des traiteurs de la zone, avec les effets d'une production de briquettes variable en temps.

La troisième variante, les équipements mobiles de briquetage, paraît être la plus appropriée aux conditions de notre pays. En effets, l'utilisation de ces équipements est justifiée par de nombreux avantages, comme:

1. Chez le traiteur de ,asse de bois:
   - L'utilisation de l'équipement de compactage seulement au besoin, au moment où l'on a réalisé la quantité suffisante de déchets qui q besoin de l'opération de compactage.
   - On évite les investissements coûteux nécessaires pour la productiondes équipements de compactage des déchets de bois.
   - On évite d'occuper l'espace avec des équipements de grandes dimensions.
   - L'obtention par compactage d'un produit performant de combustible solide, ayant des propriétés supérieures de combustion.
2. Chez le fournisseur de services de compactage de déchets de bois:
   - Possibilité de rendre service à un grand nombre de traiteurs de ,asse de bois, quelle que en soit la quantité.
   - Optimiser les déplacements chez les clients, sous l'aspet des quantités stockées de déchets de bois.
   - Optimiser le fonctionnement permanent de l'équipement et cela à parametres maximales.
   - Possibilites d'amélioration permanente de solutions constructives à partir de l'experience accu,ulée pendant l'exploitation dans de différantes conditions.
   - Valorisation du produit résulté par sa commercialisation, autant sur la ,arché interne qu'extérieur.
   - Application des standards de qualité et d'environnement au niveau européen:
3. Sous aspect écologique et social, au nivequ local et national:
   - Assurer une protection écologique efficiente de la population, de l'eau, de la forêt etc.
   - Récyclqge des matériqux.
   - Éli,iner les déchets de bois des surfaces de stockage.
   - Assurer des performances de combustion supérieures des produits briquetés, sous l'aspect d'une durée plus grande de combustion d'un même volume de materiel et d'une quantité plus grande de chaleur récupérée. Par example, on a constaté que dans un échangeur de chaleur classique on peut récupérer entre 30% et 50% de la quantité de chaleur dégagée par la combustion des bois de feu; par contre, on peut récupérer entre 50% et 80% de la quantité de chaleur dégagée par les briquettes réalisées de la même quantité du materiel de bois.
   - Eviter le déboisement noncontrôlé de la forêt dans des buts énergétiques, en faisant ainsi des économies.

Utiliser d'une manière efficiente des déchets de bois résultés à la suite du traitement du bois.

- Réduire le volume de stockage des ,atériaux combustible, tenant compte du fait que le volume d'une briquett et d'environ sept-huit fois plus réduit que le volume occupé par la même quantité de sciure avant le briquetage.
- Réaliser une alternative simple pour la production de la chaleur ménagère ou dans des entreprise de petite industrie.
- Réaliser de nouveaux emplois.
- Urgenter l'harmonisation des lois dans le domaine de l'écologie de notre pays avec celles européennes.

De l'analyse ci-dessus résulte que la ,eilleure solution pour éliminer les déchets de sciure est la réalisation de certains équipments mobiles de séchement et compactage. Une telle solution envisage de monter l'équipement mobile de séchage ey compactage sur des plateformes déplaçables (remorques, camions etc): Cela est un élément de nouveauté par l'activité dans le domaine.

3. PROJECTION DE L'ÉQUIPEMENT DE SÉCHAGE-COMPACTAGE

Les éclats de bois et la sciure présentent après le débitage une humidité élevée, corespondant à l'espèce de bois d'où proviennent (humidité minimale 30%...40%). Pour réaliser le processus technologique de compactage il est nécessaire de sécher la sciure. Le processus de séchage, qui représente la première étape de la chaîne technologique, est déter,iné par la dimension des particules de sciure, c'est à dire leur surface apparente.

Après séchage, les éclats de bois et de sciure sont compactés sous forme de briquettes utilisables dans des buts énergetiques, pour le réchauffement et la préparation de la nourriture.

L'instalation mobile de séchage et compactage de la sciure, qui peut être transportée chez différents utilisateurs, là où il est nécessaire, diminuant ainsi les investissements imposés par le processus technologique, contribuant aussi à la réduction de la pollution dans le domaine, est présentée dans la figure 1.

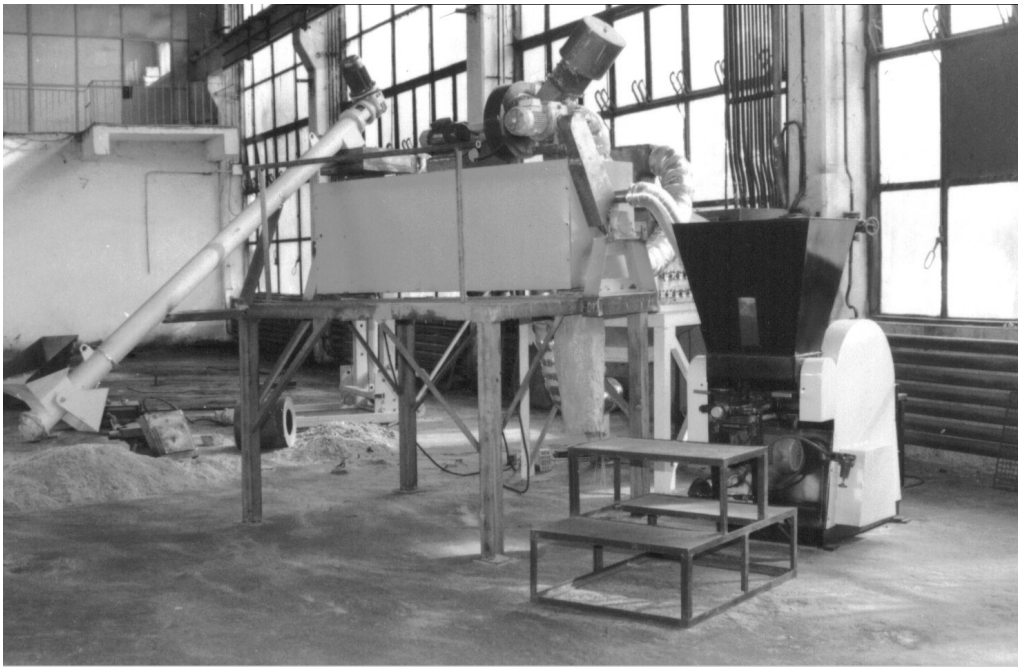

Fig. 1. Installation expérimentale pour le compactage de la sciure

Le principal élément de l'installation, qui a nécessité une attention particulière au moment de la projection, a été le sécheur.

En général, on peut classifier les méthodes de séchage, et les équipements de séchage, d'après la manière dans laquelle la chaleur est transmise vers le corps sou,is au séchage, la manière dont l'humidité du matériel est enlevée, du régime de travail, de l'agent de séchage utilisé etc. Tous ces aspects, avec la grande variété de produits sou,is au séchage et avec la li,ite supérieure de la température maximale admise, mènent à une grande variété de solutions constructives pour les sécheurs. La plus utilisée solution constructive dans le domaine emploie autant le transfert conductif, que celui convectif de chaleur [1, 2]. Ces équipements peuvent utiliser comme agent de séchage soit l'air chaud, soit les gaz de combustion [3,4].

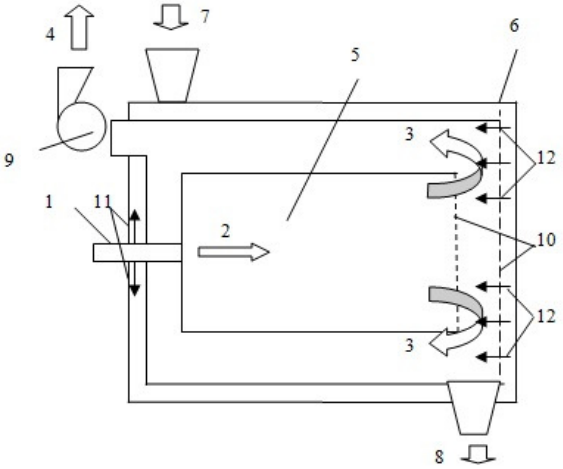

Fig. 2. Solution constructive 1. conduit pour l'agent de séchage; 2. entrée de l'agent de séchage; 3. retour de l'agent de séchage; 4. sortie de l'agent de séchage; 5. tambour intérieur; 6. tambour extérieur; 7.introduction du matériel humide; 8. évacuation du matériel sec; 9. exhaustor; 10. tamis de filtration; 11. entrée de l'agent de séchage dans le tambour extérieur; 12. sortie de l' agent de séchage du tambour extérieur

Pour l'installation mobile conçue, on a opté pour un sécheur à rotor thermique [5], dont le schéma est présenté dans la figure 2.

La solution constructive du sécheur, choisi après une attentive et minutieuse analyse des conditions complexes exigées, est la suivante: sécheur rotatif équipé de lames de mélange et utilisant un mécanisme combiné de transfert de chaleur conductif et convectif, ayant aussi une componente radiante . Comme agent de séchage on a pris en considération autant l'air chaud que les gaz de combustion, la décision finale sera prise après quelques expérimentes pratiques.

La circulation de l'agent de séchage se fera d'abord par l'intérieur de l'installation, pour chauffer la surface qui entre en contact avec le matériel, pour entrer après directement en contact avec le matériel, touchant ainsi les deux buts: séchage du matériel et enlèvement de l'humidité.

Le tambour extérieur est équipé d'un mécanisme de rotation. Ce mouvement assure un contact supérieur entre le matériel et les parois du sécheur, permettant ainsi l'amélioration du transfert de chaleur conductif, évitant en même temps la formation des dépôts de matériel, qui pourrait perturber le processus de séchage.

4. CONCLUSIONS

L'utilisation d'une installation mobile d'élimination des déchets résultés par le traitement du bois a une importance particulière pour notre pays, où l'exploitation du bois est intense, mais où l'on néglige les aspects d'écologisation. En même temps, on évite le déboisement non contrôlé de la forêt dans des buts énergétiques, épargnant ainsi la masse de bois destinée à la combustion et on assure une utilisation plus efficiente des déchets de bois résultés après le travail du bois. Donc, ce type d'installation présente des avantages, autant du point de vue d'un traitement écologique des déchets que du point de vue de l'élimination du bois primaire dans les processus de combustion, par l'utilisation dans ces processus des briquettes obtenues par le compactage des déchets.

De plus, l'utilisation d'une installation mobile, qui permet le déplacement, s'il est nécessaire, vers de divers utilisateurs, présente de multiples avantages, technologiques et économiques à la fois.

REFERENCES

[1]Krischer, O., *Die Wissenschaftlichen Grundlagen der Trocknungstechnik*, Springer Verlag, Berlin, 1978.

[2] Dăscălescu, A., *Uscarea şi aplicaţiile ei industriale,* Editura Tehnică, Bucureşti, 1964.

[3] Mujumdar, A. S., *Handbook of Industrial Drying*, 3rd Ed, CRC Press, New York, 2006.

[4] Tsotsas, E., Mujumdar, A. S., *Modern Drying Technology*, Wiley & Son, Weinheim, 2007.

[5] Răducanu, P., *Aspects Regarding the Design of a Rotary Dryer for an Equipment which Compresses Sawdust,* pp 233-243, Buletinul Institutului Politehnic din Iasi, tom LVI(LX) 2010

THERMODYNAMIC OPTIMIZATION MODEL OF AN ENDO- AND EXOIRREVERSIBLE SINGLE STAGE VAPOUR COMPRESSION REFRIGERATION SYSTEM

Horaţiu POP[1], Gheorghe POPESCU[1], Michel FEIDT[2] ,
Nicolae BĂRAN[1], Valentin APOSTOL[1], Cristian Gabriel ALIONTE[1]

[1] UNIVERSITATEA "POLITEHNICA" DIN BUCUREŞTI, România.
[2] LEMTA, POLYTECHNIC INSTITUTE OF LORENA, "HENRI POINCARÉ" UNIVERSITY NANCY, France.

Rezumat. În lucrare este prezentat un model de optimizare pe baza termodinamicii proceselor ireversibile a unei instalaţii frigorifice cu comprimare mecanică de vapori (IFV) într-o singură treaptă. Modelul ia în considerare ciclul teoretic al IFV neglijând procesele de supraîncălzire şi de subrăcire. Pentru o conductanţă termică totală impusă (dimensiuni finite), modelul de optimizare ţine cont de ireversibilităţile externe determinate de transferul de căldură la diferenţă finită de temperatură dintre agentul frigorific şi cele două surse de căldură. Ireversibilităţile interne considerate sunt cele ale proceselor de comprimare şi de laminare precum şi cele ale bilanţului entropic al unui ciclu termodinamic endoireversibil. Modelul realizat permite efectuarea unui studiu de sensibilitate a coeficientului de performanţa frigorifică *COP* al IFV în funcţie de parametrii constructivi (conductanţele termice ale celor două schimbătoare de căldură considerate – vaporizator şi condensator). Considerând proprietăţile termofizice ale diferiţilor agenţi frigorifici, pentru valori impuse temperaturilor surselor şi puterii frigorifice, modelul permite optimizarea distribuţiei conductanţelor termice şi respectiv a diferenţelor de temperatură, asigurându-se o valoare maximă a coeficientului de performanţă frigorifică, respectiv un regim de funcţionare economic. Modelul de optimizare permite stabilirea influenţei tipului de agent frigorific folosit asupra regimului de funcţionare economic al IFV-urilor.
Cuvinte cheie: termodinamica proceselor ireversibile, optimizare, sisteme frigorifice, conductanţe termice, coeficient de performantă frigorifică, agenţi frigorifici.

Abstract. The paper presents a thermodynamic optimization model of an endo- and exoirreversible single stage vapour compression refrigeration system (VCRS). The model refers to the theoretical thermodynamic cycle of the single stage VCRS without superheating and subcooling processes. For an imposed value for the overall thermal conductance (finite-size constraint), the optimization model takes into account the external irreversibility due to heat transfer at finite temperature difference between the refrigerant and the heat sources. The internal irreversibility is due to the imperfection of compression and expansion processes and also to the entropic balance for an endoirreversible thermodynamic cycle. A sensitivity study has been carried out for the single stage VCRS, as well as cooling efficiency with respect to constructive parameters (thermal conductance of the heat exchangers – evaporator and condenser). Taking into consideration the thermophysical properties of different refrigerants, for imposed heat sources temperatures and cooling capacity, the model allows the optimization of the thermal conductance distribution and temperature differences which lead to a maximum cooling efficiency and to the economical functional regime, respectively. The optimization model allows establishing the influence of different refrigerants on the economical functional regime.
Keywords: irreversible thermodynamics processes, optimization, refrigeration systems, thermal conductances, cooling efficiency, refrigerants.

1. INTRODUCTION

The irreversible thermodynamics processes offers very useful means and tools for the analysis of real processes from the thermodynamic cycles of the thermal systems subjected to constraints of finite-size and finite-time interaction. The first thermodynamic cycles investigated were the two reservoirs endoreversible Carnot cycle (direct or reversed) with two kind of external irreversibility due to the heat exchange processes which occur in finite-time and at finite temperature differences between the working fluid and heat sources [1, 2].

Regarding the two reservoirs refrigeration endoreversible Carnot cycles, the first works have been conducted in order to find the optimal design parameters by involving a finite-size constraint

under the form of a total imposed heat transfer surface [3] or an imposed total thermal conductance [4], in conditions of imposed useful effect, aiming a maximum cooling efficiency (COP). In the latter work [4], the irreversibility due to a heat leak between the ambiance and the refrigerated space has been taken supplementary into consideration. Results show that the optimal design parameters correspond to the equipartition principle of the total thermal conductance.

In order to obtain results closer to real operating conditions, in the thermodynamic analysis additionally internal irreversibility have been taken into consideration. Based on this endo- and exoirreversible approach of the bithermal Carnot cycle many papers which deal with the optimization of refrigeration or heat pump systems have been published [5, 6, 7]. Similarly to the endoreversible models, all these endo- and exoirreversible models, at imposed useful effect and at finite-size constraints, point out the optimal constructive and functional parameters which lead to a maximum COP. Here, due to the endoirreversibility, the equipartition principle for heat transfer conductances is no longer fulfilled.

For a real working fluid, due to the expansion and the compression processes which take place in the saturated humid-vapour area, it is not possible to achieve a bithermal refrigeration system based on the endo- and exoirreversible Carnot cycle. Moreover, the type of the working fluid (refrigerant) has an important influence on the refrigeration system performances. Thus, there are known some endoreversible [8] or endo- and exoirreversible [9, 10] thermodynamic analysis which consider the thermophysical properties of the refrigerant.

2. OPTIMIZATION MODEL

The present paper deals with a thermodynamics optimization model for an endo- and exoirreversible single stage vapour compression refrigeration system (VCRS), without considering the superheating and subcooling processes. The optimization model takes into consideration the external irreversibility due to the heat transfer at finite temperature difference refrigerant - heat sources. The internal irreversibility is due to the imperfection of the expansion and compression processes and also to the entropic balance for an endoirreversible thermodynamic cycle. In order to obtain results closer to real operating conditions, additionally to external and internal irreversibility sources, the proposed optimization model takes into consideration the thermophysical properties of the refrigerant. So, the influence of the refrigerant type on the system performances can be investigated.

The thermodynamic optimization model is developed in conditions of finite-size constraints and imposed cooling load. The targeted functional regime is the economical one, which is characterized by the optimal constructive and functional parameters which lead to a minimum compressor power input, and respectively, a maximum cooling efficiency (COP^{max}).

The endo- and exoirreversible thermodynamic cycle for the considered single stage VCRS in T-s (temperature – mass specific entropy) diagram is presented in Fig. 1.

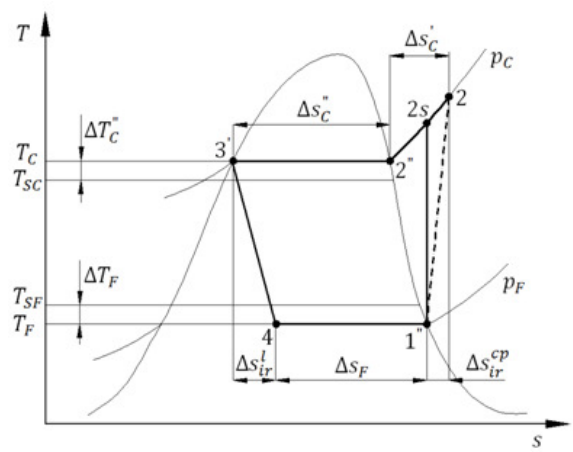

Fig. 1. The thermodynamic cycle of a single stage VCRS without subcooling and superheating in T-s diagram

For the development of the thermodynamic optimization model the following have been considered: constant temperatures of the hot and cold heat sources; steady state operation regime (constant heat and mass flow rates); the condenser is divided in two areas – one area designated with (') in which the working fluid cools down till the dry saturated vapour state (x=1) and a second area designated (") in which the condensing process takes place.

In Fig. 1 the following notations have been used:

- T_{SC} - temperature of the hot heat sink;
- T_{SF} - temperature of the cold heat source;
- T_C - condensing temperature;
- T_F - evaporating temperature;
- $\Delta T_C''$ - the temperature difference between the working fluid and the hot heat sink during the condensation process;
- ΔT_F - the temperature difference between the working fluid and the cold heat source during the evaporation process;

- Δs_F - the mass specific entropy variation during the evaporation process (4 - 1");
- Δs_{ir}^{cp} - the mass specific entropy variation during the compression process (1" - 2);
- $\Delta s_C^{'}$ - the mass specific entropy variation during the cooling process in the condenser (2 - 2");
- $\Delta s_C^{''}$ - the mass specific entropy variation during the condensation process (2" - 3');
- Δs_{ir}^{l} - the mass specific entropy variation during the expansion process (3' - 4);

2.1. Mathematical model

The mathematical model is based on the following equations:

Thermal balance equations

- at the evaporator:

$$\dot{Q}_F = K_F \cdot \Delta T_F \,;\, \Delta T_F = T_{SF} - T_F \tag{1}$$

$$\dot{Q}_F = \dot{m} \cdot q_F \,;\, q_F = h_1^{''} - h_4 \tag{2}$$

where: $\dot{Q}_F$ is the refrigeration capacity; K_F is the evaporator thermal conductance; $\dot{m}$ is the refrigerant mass flow rate; $h_1^{''}$ and h_4 are respectively, the refrigerant mass specific enthalpies at the outlet and inlet of the evaporator which give the specific thermal cooling load q_F.

- at the condenser:

$$\left|\dot{Q}_C\right| = \left|\dot{Q}_C^{'}\right| + \left|\dot{Q}_C^{''}\right| \tag{3}$$

where: $\left|\dot{Q}_C\right|$ is the heat flux rejected at the condenser; $\left|\dot{Q}_C^{'}\right|$ is the condenser heat flux rejected in the cooling area and $\left|\dot{Q}_C^{''}\right|$ is the condenser heat flux rejected during the condensing process.

$$\left|\dot{Q}_C^{'}\right| = K_C^{'} \cdot \Delta T_C^{'} \,;\, \Delta T_C^{'} = T_C^{'} - T_{SC} \tag{4}$$

where: $K_C^{'}$ is the thermal conductance corresponding to the condenser cooling area; $\Delta T_C^{'}$ is the temperature difference between the refrigerant and the hot heat sink and $T_C^{'}$ is the refrigerant mean thermodynamic temperature during the cooling process which can be computed as follows:

$$T_C^{'} = \frac{\left|\dot{Q}_C^{'}\right|}{\dot{S}_C^{'}} = \frac{\left|q_C^{'}\right|}{\Delta s_C^{'}} = \frac{h_2 - h_2^{''}}{s_2 - s_2^{''}} \tag{5}$$

in eq. (5) $\left|q_C^{'}\right|$ is the mass specific heat rejected in the condenser cooling process; h_2, s_2 and $h_2^{''}$, $s_2^{''}$ are respectively, the inlet and outlet of the condenser cooling area refrigerant mass specific enthalpies and entropies.

$$\left|\dot{Q}_C^{''}\right| = K_C^{''} \cdot \Delta T_C^{''} \,;\, \Delta T_C^{''} = T_C - T_{SC} \tag{6}$$

$$\left|\dot{Q}_C^{''}\right| = \dot{m} \cdot \left|q_C^{''}\right| \,;\, \left|q_C^{''}\right| = h_2^{''} - h_3^{'} \tag{7}$$

where: $h_2^{''}$ and $h_3^{'}$ are respectively the refrigerant mass specific enthalpies at the beginning and ending of the condensing process which give the heat rejected during the condensing process $\left|q_C^{''}\right|$.

The cycle energy balance equation is:

$$\dot{Q}_F + P_{cp} = \left|\dot{Q}_C\right| \tag{8}$$

where P_{cp} is the compressor power input which can be computed as follows:

$$P_{cp} = \dot{m} \cdot \left|l_{cp}\right| \,;\, \left|l_{cp}\right| = h_2 - h_1^{''} \tag{9}$$

The compressor outlet state can be established by defining the isentropic efficiency:

$$\eta_{is}^{cp} = \frac{T_F}{T_C} = \frac{h_{2s} - h_1^{''}}{h_2 - h_1^{''}} \Rightarrow h_2 = h_1^{''} + \frac{h_{2s} - h_1^{''}}{\eta_{is}^{cp}} \tag{10}$$

where η_{is}^{cp} can be estimated as T_F / T_C [11].

The endoirreversible cycle entropy balance equation is:

$$\frac{\dot{Q}_F}{T_F} - \left(\frac{\left|\dot{Q}_C^{'}\right|}{T_C^{'}} + \frac{\left|\dot{Q}_C^{''}\right|}{T_C} \right) + \dot{S}_{ir} = 0 \tag{11}$$

in eq. (11) $\dot{S}_{ir}$ is the entropy flux generated by the internal irreversibility and it can be written as:

$$\dot{S}_{ir} = \dot{S}_{ir}^{l} + \dot{S}_{ir}^{cp} + \dot{S}_{ir}^{\text{int}} \tag{12}$$

where: $\dot{S}_{ir}^{l}$ is the entropy flux generated during the expansion process; $\dot{S}_{ir}^{cp}$ is the entropy flux generated during the compression process and $\dot{S}_{ir}^{\text{int}}$ is the entropy flux generated by the other internal irreversibility sources in case of a endoirreversible thermodynamic cycle.

Using eq. (5), the equation (11) becomes:

$$\frac{\dot{Q}_F}{T_F} - \frac{\left|\dot{Q}_C^{''}\right|}{T_C} - \dot{S}_C^{'} + \dot{S}_{ir} = 0 \tag{13}$$

Eq. (13) can be further written as follows:

$$\frac{\dot{Q}_F}{T_F} - \frac{\left|\dot{Q}_C^{''}\right|}{T_C} + \dot{S} = 0 \tag{14}$$

where:

$$\dot{S} = -\dot{S}_C^{'} + \dot{S}_{ir} \tag{15}$$

Cooling efficiency:

$$COP = \frac{\dot{Q}_F}{P_{cp}} \tag{16}$$

The objective function of the thermodynamic optimization model is the COP maximization for imposed cooling capacity and for a total evaporator and condenser thermal conductance constraints. The aim is to find the optimal constructive configuration (thermal conductance distribution) and optimal functional conditions (refrigerant - heat source temperature differences), which lead to a maximum cooling efficiency, function of the refrigerant type used. As shown in eq. (16), in conditions of imposed cooling capacity ($\dot{Q}_F$), the maximization of the COP is achieved when the compressor power input (P_{cp}) is minimum.

Using eq. (3) and (8) the compressor power input can be written with:

$$P_{cp} = \left|\dot{Q}_C^{'}\right| + \left|\dot{Q}_C^{''}\right| - \dot{Q}_F \tag{17}$$

In order to simplify the mathematical model the heat flux rejected in the condenser cooling area can be established as a percent (pc) from the heat flux rejected during the condensing process, as follows:

$$\left|\dot{Q}_C^{'}\right| = pc \cdot \left|\dot{Q}_C^{''}\right| \tag{18}$$

So, using eq. (18), the expression (17) becomes:

$$P_{cp} = (pc+1) \cdot \left|\dot{Q}_C^{''}\right| - \dot{Q}_F \tag{19}$$

Next, the expression (19) will be processed. Starting from eq. (1) the evaporating temperature can be written as:

$$T_F = T_{SF} - \frac{\dot{Q}_F}{K_F} \tag{20}$$

Substituting eq. (20) in eq. (14) yields:

$$\frac{\dot{Q}_F}{T_{SF} - \dot{Q}_F / K_F} - \frac{\left|\dot{Q}_C^{''}\right|}{T_C} + \dot{S} = 0 \tag{21}$$

Using the eq. (6), the expression (21) becomes:

$$-\frac{K_C^{''}(T_C - T_{SC})}{T_C} + A + \dot{S} = 0 \tag{22}$$

where the following notation was used:

$$A = \frac{\dot{Q}_F}{T_{SF} - \dot{Q}_F / K_F} \tag{23}$$

From eq. (22) it results that:

$$\frac{T_{SC}}{T_C} = 1 - \frac{A + \dot{S}}{K_C^{''}} \tag{24}$$

Using the eqns. (6) and (19) the expression of compressor power input becomes:

$$P_{cp} = (pc+1) K_C^{''} T_{SC} \left(\frac{T_C}{T_{SC}} - 1 \right) - \dot{Q}_F \tag{25}$$

Substituting eq. (23) in eq. (24), eliminating T_C, and after several mathematical operations yields:

$$P_{cp} = (pc+1) T_{SC} \left(\frac{A + \dot{S}}{1 - (A + \dot{S}) / K_C^{''}} \right) - \dot{Q}_F \tag{26}$$

Based on eq. (26) the expression (16) becomes:

$$COP = \frac{1}{(pc+1) \frac{T_{SC}}{\dot{Q}_F} \left(\frac{A + \dot{S}}{1 - (A + \dot{S}) / K_C^{''}} \right) - 1} \tag{27}$$

2.2. Influence of K_F and $K_C^{''}$ on the COP

As it can be seen from eq. (27) the COP depends on the following parameters: $\dot{Q}_F$, pc, T_{SF}, T_{SC}, $\dot{S}$ and on the variables K_F and $K_C^{''}$. The values for pc, $\dot{S}$, K_F and $K_C^{''}$ are strongly influenced by the type of refrigerant being used. Thus, in order to assume appropriate values for the parameters and variables which influence the COP a program for a single stage VCRS has been developed in Engineering Equation Solver (EES) [12]. Also, in order to verify the here presented optimization model, the input data was chosen the same as in the paper [8], as follows:

$\dot{Q}_F = 80 \div 140\ kW$; $T_{SC} = 291\ K$; $T_{SF} = 268\ K$; $\Delta T_F = 6\,K$; $\Delta T_C^{''} = 8\,K$, for the refrigerant R134a.

The program developed in EES allows determining:

- the thermodynamic state parameters (pressure, temperature, quality and mass specific properties: enthalpy, entropy, volume) in all points of the single stage VCRS cycle (Fig. 1);
- $\left|\dot{Q}_C^{'}\right|$, $\left|\dot{Q}_C^{''}\right|$ and thus $\left|\dot{Q}_C\right|$;
- K_F, $K_C^{'}$, $K_C^{''}$ and the total evaporator-condenser thermal conductance K_T defined as:

$$K_T = K_F + K_C^{''} \tag{28}$$

- $\dot{S}$ and pc parameter values.

The results, obtained using the above mentioned program, are presented in Fig. 2 and Fig.3.

So, Fig. 2 shows the influence of K_F on the cooling efficiency for different cooling capacities values. As it can be seen, the cooling efficiency presents a maximum value COP^{max} corresponding to different optimum values K_F^{opt}. The value of COP^{max} is the same regardless the refrigeration capacity. One can observe that the values of K_F^{opt} are increasing with the increase of the refrigeration capacity.

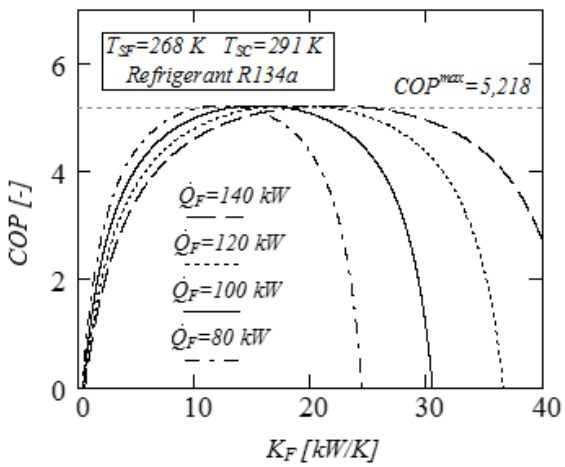

Fig. 2. COP variation with respect to K_F for different $\dot{Q}_F$

Fig. 3 gives the influence of $K_C^{"}$ on the cooling efficiency for different cooling capacities values. One can notice that a COP^{max} value is obtained corresponding to different optimum values $K_C^{"opt}$. For COP variation with respect to $K_C^{"}$ for different $\dot{Q}_F$ values it results a similar influence like in the K_F case.

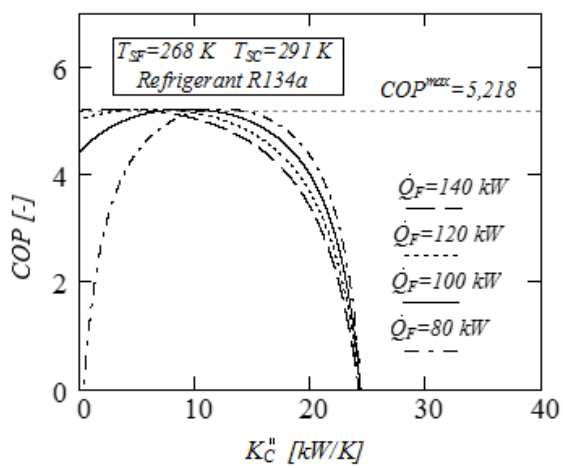

Fig. 3. COP variation with respect to $K_C^{"}$ for different $\dot{Q}_F$

As results in Fig. 2 and Fig. 3, the COP^{max} have the same value corresponding to different optimum values for K_F^{opt} and $K_C^{"opt}$.

For the optimal design of a single stage VCRS, to operate in an economical functional regime, with a minimum compressor power input at an imposed cooling capacity, and respectively, at COP^{max}, the analytical expressions for K_F^{opt} and $K_C^{"opt}$ are an important objective. These expressions will be derived next.

2.3. Analytical express. of optimal variables

To determine the analytical expressions of K_F^{opt} and $K_C^{"opt}$ the eq. (26) must be analyzed. If the values corresponding to $\dot{Q}_F$, pc, T_{SF}, T_{SC}, and $\dot{S}$ are known, then the minimum compressor power input which leads to COP^{max}, can be achieved only if the expression E is minimum.

$$E = \left(\frac{A + \dot{S}}{1 - (A + \dot{S}) / K_C^{"}} \right) \tag{29}$$

From eqns. (23) and (29) it results that the expression $E = f\left(K_F, K_C^{"}\right)$. Taking the derivate of E with respect to K_F and setting it equal to zero ($\partial E / \partial K_F = 0$), it gives the optimum thermal conductance distribution between evaporator and condenser (K_F^{opt} , $K_C^{"opt}$), corresponding to the minimum value for expression E, respectively.

It must be pointed out that the optimum thermal conductance distribution can be obtained only in condition of finite-size constraints ($K_T = ct.$), according to eq. (28).

After several mathematical computations the expression $\partial E / \partial K_F = 0$ becomes:

$$-\frac{A^2}{K_F^2} \cdot \left(1 - \frac{A + \dot{S}}{K_C^{"}}\right) - \\ -\left(A + \dot{S}\right) \cdot \frac{A^2 / K_F^2 \cdot K_C^{"} - \left(A + \dot{S}\right)}{\left(K_C^{"}\right)^2} = 0 \tag{30}$$

The expression (30) leads to:

$$\frac{A^2}{K_F^2} = \frac{\left(A + \dot{S}\right)^2}{\left(K_C^{"}\right)^2} \tag{31}$$

From eq. (31), the thermal conductance of the condenser corresponding to the condensing area can be obtained:

$$K_C^{"} = \frac{K_F \cdot \left(A + \dot{S}\right)}{A} \tag{32}$$

Using eqns. (23) and (32), $K_C^{"}$ can be written as follows:

$$K_C^{"} = K_F + \frac{\dot{S} \cdot \left(T_{SF} \cdot K_F - \dot{Q}_F\right)}{\dot{Q}_F} \tag{33}$$

Based on the finite-size constraint from eqns. (28) and (33) the optimum thermal conductance of the evaporator K_F^{opt} can be computed:

$$K_F^{opt} = \frac{K_T + \dot{S}}{2 + \dot{S} \cdot T_{SF} / \dot{Q}_F} \tag{34}$$

Substituting eq. (34) in eq. (33) yields the optimum value for the thermal conductance at the condenser in the condensing area $K_C^{"opt}$:

$$K_C^{"opt} = K_F^{opt} + \frac{\dot{S} \cdot \left(T_{SF} \cdot K_F^{opt} - \dot{Q}_F\right)}{\dot{Q}_F} \quad (35)$$

Using the eq. (28) and if in eq. (34) the term $\dot{S}$ is considered to be zero, the thermodynamic cycle is endoreversible and there is no cooling area in the condenser, then it results the well known equipartition principle [3, 4]:

$$K_F^{opt} = K_C^{"opt} = \frac{K_T}{2} \quad (36)$$

Expression (36) confirms the correctness of the here proposed thermodynamic optimization model in endoreversible case.

Substituting eqns. (34) and (35) in eqns. (26) and (27), the minimum compressor power input and maximum cooling efficiency can be written:

$$P_{cp}^{\min} = (pc+1)T_{SC}\frac{A^{opt} + \dot{S}}{1-(A^{opt} + \dot{S})/K_C^{"opt}} - \dot{Q}_F \quad (37)$$

$$COP^{\max} = \frac{1}{(pc+1)\frac{T_{SC}}{\dot{Q}_F}\frac{A^{opt} + \dot{S}}{1-\frac{A^{opt} + \dot{S}}{K_C^{"opt}}} - 1} \quad (38)$$

where $A^{opt} = \dfrac{\dot{Q}_F}{T_{SF} - \dot{Q}_F / K_F^{opt}}$ (39)

Moreover, the optimum temperature differences between the working fluid and the heat sources can be determined.

Using eqns. (1) and (34) the optimal temperature difference at the evaporator can be expressed as:

$$\Delta T_F^{opt} = \frac{\dot{Q}_F}{K_F^{opt}} \quad (40)$$

Using eqns. (19) and (37), the minimum heat flux rejected at the condenser in the condensing area can be written as:

$$\left|\dot{Q}_C^{"\min}\right| = \frac{P_{cp}^{\min} + \dot{Q}_F}{(pc+1)} \quad (41)$$

Based on eq. (6), eqns. (35) and (41), the optimal temperature difference at the condenser in the condensing area can be expressed as:

$$\Delta T_C^{"opt} = \frac{\left|\dot{Q}_C^{"\min}\right|}{K_C^{"opt}} \quad (42)$$

Furthermore the thermal conductance of the condenser in the cooling area can be determined using eq. (4):

$$K_C^{'} = \frac{\left|\dot{Q}_C^{'}\right|}{\Delta T_C^{'}} \quad (43)$$

Using eqns. (35) and (43), the optimal overall thermal conductance of the condenser can be expressed as:

$$K_C^{opt} = K_C^{"opt} + K_C^{'} \quad (44)$$

Using eqns. (3) and (44), it can be assumed that the overall optimal temperature difference at the condenser can be written as:

$$\Delta T_C^{opt} = \frac{\left|\dot{Q}_C\right|}{K_C^{opt}} \quad (45)$$

Finally, the optimal variable values lead to the economical functional regime, characterized by $COP^{\max}$, which can be synthetically expressed as:

$$parameters\left\{\begin{matrix}\dot{Q}_F \\ T_{SF} \\ T_{SC} \\ \dot{S} \\ pc \\ K_T\end{matrix}\right\} \Rightarrow optimized\ variables\left\{\begin{matrix}K_F^{opt} \\ K_C^{"opt} \\ K_C^{opt} \\ \Delta T_F^{opt} \\ \Delta T_C^{opt}\end{matrix}\right\}$$

The economical functional regime is the functional regime targeted during the design activity of single stage VCRS.

3. RESULTS

The optimal variables which give the maximum coefficient of performance are directly influenced by the type of refrigerant being used. In order to point out this influence, based on the program developed in EES the optimal variable values have been comparatively investigated taking into consideration the refrigerants R134a, R22, R12, R404A, R410A, R717, R600a and R290 for cooling capacities within the range $\dot{Q}_F = 80 \div 140\ kW$. The results are presented in a tabular manner (Table I - Table V).

Thus, Table I, presents the variation of K_F^{opt} for different refrigerants and $\dot{Q}_F$ values. As expected, K_F^{opt} increases with the increase of $\dot{Q}_F$ for all of the analyzed refrigerants. Moreover, the values of K_F^{opt} are similar for all considered refrigerants.

Table II presents the variation of $K_C^{"opt}$ for different refrigerants and $\dot{Q}_F$ values. Compared to K_F^{opt}, $K_C^{"opt}$ presents different values for the analyzed refrigerants. Thus, refrigerant R717 leads to the smallest value for $K_C^{"opt}$, whilst refrigerant R600a leads to the biggest value. Comparable

values for $K_C^{"opt}$ are obtained for the refrigerant pairs R134a – R12, and R404A – R290. But, for all refrigerants it results that the values for $K_C^{"opt}$ increase with the increase of $\dot{Q}_F$.

Table 1

K_F^{opt} for different refrigerants and $\dot{Q}_F$

	K_F^{opt} $[kW/K]$			
$\dot{Q}_F$ $[kW]$	R134a	R22	R12	R404A
80	12.37	12.32	12.38	12.37
100	15.47	15.49	15.47	15.47
120	18.56	18.59	18.57	18.56
140	21.66	21.69	21.66	21.65
$\dot{Q}_F$ $[kW]$	R410A	R717	R600a	R290
80	12.40	12.41	12.36	12.37
100	15.50	15.51	15.45	15.47
120	18.60	18.61	18.54	18.56
140	21.70	21.71	21.63	21.66

Table 2

$K_C^{"opt}$ for different refrigerants and $\dot{Q}_F$

	$K_C^{"opt}$ $[kW/K]$			
$\dot{Q}_F$ $[kW]$	R134a	R22	R12	R404A
80	12.29	11.67	12.21	12.38
100	15.36	14.59	15.27	15.48
120	18.43	17.51	18.32	18.57
140	21.50	20.42	21.37	21.67
$\dot{Q}_F$ $[kW]$	R410A	R717	R600a	R290
80	11.38	11.21	12.78	12.30
100	14.23	14.01	15.98	15.37
120	17.08	16.81	19.18	18.45
140	19.92	19.61	22.37	21.52

Table 3

ΔT_F^{opt} for different refrigerants and $\dot{Q}_F$

	ΔT_F^{opt} $[K]$			
$\dot{Q}_F$ $[kW]$	R134a	R22	R12	R404A
80	6.47	6.46	6.46	6.47
100	6.47	6.46	6.46	6.47
120	6.47	6.46	6.46	6.47
140	6.47	6.46	6.46	6.47
$\dot{Q}_F$ $[kW]$	R410A	R717	R600a	R290
80	6.45	6.45	6.47	6.47
100	6.45	6.45	6.47	6.47
120	6.45	6.45	6.47	6.47
140	6.45	6.45	6.47	6.47

Table III and Table IV present the optimal temperature differences at the evaporator and the condenser in the condensing area for different refrigerants and $\dot{Q}_F$ values. As it can be seen, the values for ΔT_F^{opt} and $\Delta T_C^{"opt}$ are very close regardless the type of refrigerant and are the same for a given cooling capacity and a certain type of refrigerant. The results presented in Table III and Table IV are in good concordance with the those published in [8, 9].

Table 4

$\Delta T_C^{"opt}$ for different refrigerants and $\dot{Q}_F$

	$\Delta T_C^{"opt}$ $[K]$			
$\dot{Q}_F$ $[kW]$	R134a	R22	R12	R404A
80	7.38	7.36	7.37	7.38
100	7.38	7.36	7.37	7.38
120	7.38	7.36	7.37	7.38
140	7.38	7.36	7.37	7.38
$\dot{Q}_F$ $[kW]$	R410A	R717	R600a	R290
80	7.36	7.36	7.38	7.38
100	7.36	7.36	7.38	7.38
120	7.36	7.36	7.38	7.38
140	7.36	7.36	7.38	7.38

Table 5

$COP^{\max}$ for different refrigerants and $\dot{Q}_F$

	$COP^{\max}$ $[-]$			
$\dot{Q}_F$ $[kW]$	R134a	R22	R12	R404A
80	5.22	5.25	5.30	4.83
100	5.22	5.25	5.30	4.83
120	5.22	5.25	5.30	4.83
140	5.22	5.25	5.30	4.83
$\dot{Q}_F$ $[kW]$	R410A	R717	R600a	R290
80	5.08	5.35	5.23	5.16
100	5.08	5.35	5.23	5.16
120	5.08	5.35	5.23	5.16
140	5.08	5.35	5.23	5.16

Table V shows the variation of $COP^{\max}$ for different refrigerants and $\dot{Q}_F$ values. For a certain type of refrigerant the values for $COP^{\max}$ are the same regardless the cooling capacity. The refrigerant R717 leads to highest value for $COP^{\max}$ among the analyzed refrigerants, whilst R404A leads to the smallest value. Close values for $COP^{\max}$ are obtained for refrigerants R134a, R12 and R22. Between refrigerants R600a and R290, the highest value for $COP^{\max}$ is obtained for R600a. The results presented in Table V are also in good correlation with the results published in papers [8, 9].

4. CONCLUSIONS

The paper presents a thermodynamic optimization model of an endo- and exoirreversible single stage vapour compression systems (VCRS) without superheating and subcooling processes. The external irreversibility is due to heat transfer between the working fluid and heat sources at

finite temperature differences. The internal irreversibility is due to the imperfection of the expansion and compression processes, considering the entropic balance for the endoirreversible thermodynamic cycle and also to the thermodynamic properties of the real working fluid.

The optimization model has been developed based on heat exchangers (evaporator and condenser) thermal balance equation and energy and entropy thermodynamic cycle balance equations. In finite-size constraints (constant heat exchanger total thermal conductance) and imposed cooling load conditions, the aim is to find the optimal constructive configuration (thermal conductance distribution) and optimal functional conditions (refrigerant - heat source temperature differences), which lead to a maximum cooling efficiency (COP), function of the refrigerant type used.In a first part, the existence of an economical operating regime, characterized by a maximum value for the COP with respect to the thermal conductance of the evaporator has been demonstrated. The maximum value of the COP is the same regardless the cooling capacity, but for different thermal conductance distributions. The values of the parameters and variables which have a direct influence on the COP and the compressor power input have been determined based on a program developed for a single stage VCRS in Engineering Equation Solver for refrigerant R134a. In order to validate the results of the here proposed thermodynamic model, the input data has been chosen in accordance with another similar published papers.In a second part, the expression of the optimal variables has been determined analytically. Furthermore, based on the program developed in EES the influence of the refrigerant type being used on the optimal variable values has been pointed out. The investigated refrigerants are R134a, R22, R12, R404A, R410A, R717, R600a and R290 for cooling capacities within the range $\dot{Q}_F = 80 \div 140\,kW$.

The results have been comparatively presented in a tabular manner; they are in good concordance with the considered references.The main advantage of the presented optimization model is its simplicity and the fact that it allows to point out the influence of the refrigerant being used on the variables which give the COP^{max}. At the same time the optimization model gives valuable information regarding the economical operating regime, which is the targeted functional regime during the design activity for single stage VCRS. The optimization model can be improved by taking into consideration also the superheating and subcooling processes. The results obtained this way should give information closer to real operating conditions of single stage VCRS.

REFERENCES

[1] Curzon, F.L., Ahlborn, B., *Efficiency of Carnot engine atmaximum power output*. Am. J. Phys., Vol. 43, pp. 22-24, (1975).

[2] Blanchard, C.H., *Coefficient of performance for finite speed heat pump*. J. Appl. Phys., Vol. 51, pp. 2471-2472, (1980).

[3] Goth, Y., Feidt, M., *Conditions optimales de fonctionnement des pompes à chaleur ou machines á froid associées à un cycle de CARNOT endoreversible*, C.R.A.S., 303, Series II, (1986).

[4] Bejan, A., T*heory of heat transfer irreversible refrigeration plants*, Int. J. Heat Mass Transfer, Vol. 32, no. 9, pp. 1631-1639, (1989).

[5] Popescu G., Pop H., Apostol V., *Irreversible Thermodynamics Analyze of single stage VCRS economic-ecologic functional regimes* (in Romanian), Proc. of the XIV-in SRT Conference, Volume on CD, UTCB Edition, paper C29, Bucharest, 25-26 November, (2004).

[6] Vasilescu E., Radcenco V., Popescu G., *Design Optimization of Vapor Compression Chillers based on Finite Time Thermodynamics*, Proc. of Int. Conf. ECOS'96, pp. 153-156, Stockolm, Sweden, (1996).

[7] Pop H., Feidt M., Popescu G., Apostol V., Alionte C.G., *Optimization of conventional Irreversible Cascade Refrigeration System*, "Politehnica" University of Bucharest Scientific Bulletin, Series D (Mechanical Engineering), Vol. 71 (4), pp. 17-28, (2009).

[8] Grosu L., Radcenco V., Feidt M., *Benelmir R., Thermodynamique en temps fini de machines à production de froid et de chaleur à deux réservoirs. Comparaison avec l`approche thermoéconomique*, Termotehnica Revue, no. 1, pp. 13-25, (2002).

[9] Vasilescu E.E., *Optimization Researches of the Complex Schemas in Air Conditioning* (in Romanian), PhD thesis, "Politechnica" University of Bucharest, (1999).

[10] Vasilescu E.E., Dobrovicescu Al., Radcenco V., Soloiu V., *Finite Time and Dimension Analysis of the Two Heat Sources Refrigeration Systems*, ECOS'02, Vol. III, p.p. 1485-1491, Berlin, Germany, (2002).

[11] Popescu G., Apostol V., Porneală S. et. al., *Equipment and Frigorific Plants* (in Romanian), Printech Edition, (2005).

[12] Klein S.A., Engineering Equation Solver Software, Academic Commercial version V8.646 (08/16/10), #2538, (2010).

SPECTRAL RESPONSE OF NON-LINEAR MECHANICAL SYSTEMS UNDER RANDOM EXCITATION

Marinică STAN [1], Petre STAN[2]

[+]UNIVERSITY OF PITEŞTI, Romania.
[++]METALLURGICAL HIGH SCHOOL, Slatina, Romania.

Rezumat. Lucrarea dezbate o metodă pentru determinarea densităţii spectrale de putere a răspunsului la excitaţii aleatoare de bandă largă cu zgomot alb ale unui oscilator neliniar. Funcţia densitate de probabilitate se obţine cu ajutorul metodei liniarizării echivalente. Metoda de liniarizare a sistemului neliniar stochastic se bazează pe faptul că un sistem neliniar poate fi înlocuit cu un sistem liniar prin reducerea la minimum a erorii introduse prin liniarizare între cele două sisteme. Apoi se realizează estimarea spectrului de răspuns. Această estimare se face prin aflarea densităţii spectrale de putere a răspunsului folosindu-se densitatea de probabilitate a sistemului. Eficienţa metodei constă în compararea rezultatelor cu cele obţinute prin simulări numerice.
Cuvinte cheie: vibraţie aleatoare, funcţia densitate spectrală, răspuns.

Abstract. A method for estimating the power spectral density of the stationary response of oscillator with a nonlinear restoring force subjected to external wide band noise excitation has been proposed. The probability density function is obtained using the equivalent linear principle. The method of the stochastic equivalent linearization is based on the idea that a nonlinear system may be replaced by a linear system by minimizing the mean square error of the two systems. Next, an estimate of the non-linear response spectrum is derived providing the expectation of the spectral density function of the random spring system with respect to the probability density function The efficiency of the method is checked by comparing results with those numerical simulations.
Keywords: random vibration, spectral density function, response.

1. SYSTEM MODEL

To illustrate the procedure of equivalent linearization theory, let us consider the following oscillator with a nonlinear restoring force component .The ordinary differential equation of the motion can be written as:

$$m\ddot{\eta}(t) + c\dot{\eta}(t) + g(\eta(t)) = F(t)\,, \qquad (1)$$

where m is the mass, c is the viscous damping coefficient, $F(t)$ is the external excitation signal with zero mean and $\eta(t)$ is the displacement response of the system.
Dividing the equation by m, the equation of motion can be rewritten as:

$$\ddot{\eta}(t) + 2\xi p\dot{\eta}(t) + h(\eta(t)) = f(t)\,, \qquad (2)$$

where ξ is the critical damping factor, and p is the undamped natural frequency, for the linear system.

We can always find a way to decompose the nonlinear restoring force to one linear component plus a nonlinear component

$$h(\eta) = p^2(\eta + G(\eta)\alpha)\,, \qquad (3)$$

where α is the nonlinear factor to control the type and degree of nonlinearity in the system. The idea of linearization is replacing the equation by a linear system:

$$\ddot{\eta}(t) + 2\xi_e p_e\dot{\eta}(t) + p_e{}^2\eta(t) = f(t), \qquad (4)$$

where

$$\xi_e = \frac{p}{p_e}\xi \qquad (5)$$

is the damping ratio of equivalent linearized system and p_e is the natural frequency of the equivalent linearized system.

To find an expression for p_e , it is necessary to minimize the expected value of the difference

between equations (2) and (4) in a least square sense. Now the difference is the difference between the nonlinear stiffness and linear stiffness terms, which is

$$e = h(\eta(t)) - p_e^2 \eta(t) \tag{6}$$

The value of p_e can be obtained by minimizing the expectation , of the square error:

$$\frac{dE\{e^2\}}{dp_e^2} = 0 . \tag{7}$$

Substituting the equation (6) into equation (7) performing the necessary differentiation, the expression of p_e can be obtained as:

$$p_e^2 = p^2 (1 + \alpha \frac{E\{\eta G(\eta)\}}{\sigma_\eta^2}) , \tag{8}$$

where σ_η is the standard deviation of $\eta(t)$. This equation shows how the nonlinear component of the stiffness element affects the value of p_e.

The displacement variance [1,2,3] of the system under Gaussian white noise excitation can be expressed as,

$$\sigma_\eta^2 = R_\eta(0) = \int_{-\infty}^{\infty} \left| H(\omega) \right|^2 S_F d\omega , \tag{9}$$

where the frequency response function of the single degree of freedom system is

$$\left| H(\omega) \right| = \frac{1}{m\sqrt{(p_e^2 - \omega^2)^2 + 4\xi_e^2 p_e^2 \omega^2}} . \tag{10}$$

In equation (8), the exact evaluation of $\frac{E\{\eta G(\eta)\}}{\sigma_\eta^2}$ requires knowledge of the first-order density function of the response process $\eta(t)$.

The spectral density of the response is given by:

$$S_\eta(\omega) = \frac{S_F(\omega)}{m^2[(p_e^2 - \omega^2)^2 + 4\xi_e^2 p_e^2 \omega^2]} . \tag{11}$$

We obtain:

$$S_\eta(\omega) = \frac{1}{m^2} \frac{S_F(\omega)}{u^2 + 4\xi_e^2 p^2 \omega^2 (1 + \frac{6\alpha\sigma_\eta^2}{\sqrt{\pi}} \Gamma(\frac{3}{2}))} , \tag{12}$$

where

$$u = p^2 - \omega^2 + \frac{6\alpha p^2 \sigma_\eta^2}{\sqrt{\pi}} \Gamma(\frac{3}{2}) . \tag{13}$$

$S_\eta(\omega)$ and $S_F(\omega)$ are the power spectral density for $\eta(t)$ and $F(t)$ respectively.

2. EXAMPLE: THE SPECTRAL ANALYSIS OF A SINGLE STORY BUILDING UNDER RANDOM LOAD

A single-story building is modeled by four identical columns of Young's modulus E and height h and a rigid floor of weight m. The damping can be approximated by an equivalent damping constant c. The ground acceleration due to an earthquake is assumed to be a Gaussian white noise with a constant spectrum S_0 .The columns have cilinder sections of diameter D.

The moment of inertia I for the columns [1] and the total stiffness of the four columns k are:

$$I = \frac{\pi D^4}{64} , \tag{14}$$

$$k = \frac{3nEI}{h^3} . \tag{15}$$

Note that as the ground acceleration is assumed to be a Gaussian white noise of constant spectral density S'_0 , the spectral density [4,5,6] of the earthquake force that acts on the structure can be found to be $(0,5...1,1)m^2 S'_0$. This can be readily seen from the definition of spectral density function which is the Fourier transform of the autocorrelation function.

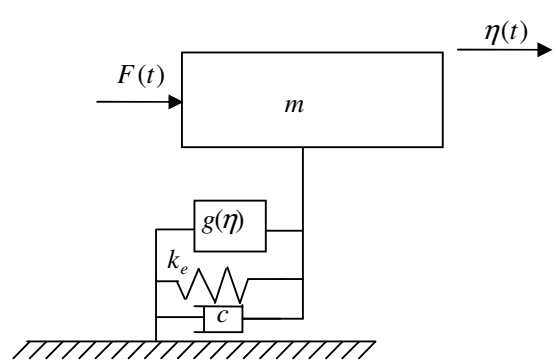

Fig. 1. Spectral analysis of a SDOF system under random-load.

The equation of motion for this single-degree of freedom structure under earthquake excitation can be written as,

$$m\ddot{\eta}(t)+c\dot{\eta}(t)+g(\eta(t))=-m\ddot{\eta}_g(t), \quad (16)$$

where m is the mass, c is the viscous damping coefficient, $F(t)=m\ddot{\eta}_g(t)$ is the external excitation signal with zero mean and $\eta(t)$ is the displacement response of the system.

Dividing the equation by m, the equation of motion can be rewritten as:

$$\ddot{\eta}(t)+2\xi p\dot{\eta}(t)+h(\eta(t))=-\ddot{\eta}_g(t), \quad (17)$$

where ξ is the critical damping factor, and p is the undamped natural frequency, for the nonlinear system.

$$\ddot{\eta}(t)+2\xi_e p_e\dot{\eta}(t)+p_e^2\eta(t)=w(t), \quad (18)$$

where

$$\xi_e=\frac{p}{p_e}\xi. \quad (19)$$

is the damping ratio of equivalent linearized system and p_e is the natural frequency of the equivalent linearized system.

The displacement variance of the single-degree of freedom system under Gaussian white noise excitation can be expressed [2] as,

$$\sigma^2_\eta=R_\eta(0)=\int_{-\infty}^{\infty}\left|H(\omega)\right|^2 S_F d\omega= =\int_{-\infty}^{\infty}\left|H(\omega)\right|^2 mS_{\ddot{\eta}_g} d\omega \quad (20)$$

where the frequency response function of the system is,

$$\left|H(\omega)\right|=\frac{1}{\sqrt{(p_e^2-\omega^2)^2+4\xi_e^2 p_e^2\omega^2}}. \quad (21)$$

The most used spectrum to describe the earthquake ground accleration is earthquake spectrum [3,4]

which is expresses as $S_{\ddot{\eta}_g}=mS'_0$, where

$$S'_0=(0,5...1,1)\frac{m^2}{s^3}, \quad (22)$$

Obtain

$$\sigma^2_\eta=S'_0\pi\frac{1}{2\xi_e p_e^3}=\frac{S'_0\pi}{2\xi pp_e^2}= =\frac{S'_0\pi}{2\xi p^3\left(1+\frac{\alpha E\{\eta G(\eta)\}}{\sigma^2_\eta}\right)}. \quad (23)$$

The velocity variance of the system can be expressed as,

$$R_{\dot{\eta}}(\tau)=-\frac{d^2R_\eta(\tau)}{d\tau^2}=\int_{-\infty}^{\infty}\omega^2\bar{S}_\eta(\omega)e^{i\omega\tau}d\omega. \quad (24)$$

Obtain for the velocity variance

$$\sigma^2_{\dot{\eta}}=E\{\dot{\eta}^2\}=R_{\dot{\eta}}(0)=\int_{-\infty}^{\infty}\omega^2 S_\eta(\omega)d\omega= =S'_0m^2\int_{-\infty}^{\infty}\frac{\omega^2}{m[(p_e^2-\omega^2)^2+4\xi^2p^2\omega^2]}d\omega= =\frac{S'_0\pi}{2\xi p}=\frac{\pi S'_0m}{c}. \quad (25)$$

The relative acceleration of this structure is unbounded. On the other hand, the absolute acceleration $\ddot{\eta}_{abs}$ is bounded and can be obtained as follows:

$$\ddot{\eta}_{abs}=\ddot{\eta}(t)+\ddot{\eta}_g(t)=2\xi_e p_e\dot{\eta}(t)+p_e^2\eta(t). \quad (26)$$

Taking the mean [5,6] value of (26) the square of leads to

$$E\{\ddot{\eta}^2_{abs}\}=4\xi_e^2p_e^2E\{\dot{\eta}^2(t)\}+ +p_e^4E\{\eta^2(t)\}+4\xi_e p_e^3E\{\dot{\eta}(t)\eta(t)\}. \quad (27)$$

As

$$E\{\dot{\eta}(t)\eta(t)\}=0, \quad (28)$$

(27) can be further written as,

$$\sigma^2_{\ddot{\eta}_{abs}}=4\xi_e^2p_e^2\sigma^2_{\dot{\eta}}+p_e^4\sigma^2_\eta=\frac{\pi S'_0c}{m}+ +\frac{\pi S'_0mp_e^2}{c}=\pi S'_0\left(\frac{c}{m}+\frac{mp_e^2}{c}\right) \quad (29)$$

The spectral density of the response is given by:

$$S_\eta(\omega)=\frac{S_F}{m^2}\frac{1}{A^2+4\xi^2p^2\omega^2}, \quad (30)$$

where

$$A = p^2 + \frac{p^2 ck\alpha E\{\eta(t)G(\eta(t))\}}{\pi S'_0 m^2 - ck\alpha E\{\eta(t)G(\eta(t))\}} - \omega^2 . \quad (31)$$

3. NUMERICAL RESULTS

In this example, $S'_0 = 0,52\frac{m^2}{s^3}$, $m = 2\cdot 10^5 kg$, n=4 columns, $d = 0,5m$, $h = 2m$, $E_b = 0,2\cdot 10^{11} Pa$, $\xi = 0,25$, $G(\eta) = \eta^5(t)$, $\alpha = 2,91\cdot 10^4 m^{-4}$.

The power spectral density for excitation $S_F(\omega)$ is $S_F(\omega) = m^2 S'_0 = 2,08\cdot 10^{10} N^2 \cdot s$.

The equation of motion for this single-degree of freedom structure under earthquake excitation can be written as,

$$\ddot{\eta}(t) + 2\xi p\dot{\eta}(t) + p^2\eta(t) + \alpha p^2\eta^5(t) = -\ddot{\eta}_g(t) . \quad (32)$$

Obtain:

$$k = 29\cdot 10^6 \frac{N}{m}; \quad p = 12,04 s^{-1}; \quad c = 1204\cdot 10^3 \frac{N\cdot s}{m}, \quad (33)$$

$$E\{\eta(t)G(\eta(t))\} = E\{\eta^6(t)\} = \int_{-\infty}^{\infty} \eta^6 \frac{e^{-\frac{\eta^2}{2\sigma_\eta^2}}}{\sigma_\eta\sqrt{2\pi}} d\eta =$$

$$= \frac{1}{\sigma_\eta\sqrt{2\pi}} \int_{-\infty}^{\infty} \eta^6 e^{-\frac{\eta^2}{2\sigma_\eta^2}} d\eta = \frac{(\sigma_\eta\sqrt{2})^6}{\sqrt{\pi}} \int_{-\infty}^{\infty} u^6 e^{-u^2} du = \quad (34)$$

$$= \frac{(\sigma_\eta\sqrt{2})^6}{\sqrt{\pi}} \left[-\frac{1}{2} e^{-u^2} u^5 \Big|_{-\infty}^{\infty} + \frac{5}{2} \int_{-\infty}^{\infty} u^4 e^{-u^2} du \right] =$$

$$= \frac{5(\sigma_\eta\sqrt{2})^6}{2\sqrt{\pi}} \int_{-\infty}^{\infty} u^4 e^{-u^2} du = 5\sigma^2 E\{\eta^4\}$$

where

$$u = \frac{\eta}{\sigma_\eta\sqrt{2}}, \quad (35)$$

and

$$E\{\eta^4\} = 3\sigma^2 E\{\eta^2\} . \quad (36)$$

Obtain

$$E\{\eta(t)G(\eta(t))\} = E\{\eta^6(t)\} = 15\sigma^6_\eta . \quad (37)$$

By substitution (37) in the (23) we obtain:

$$15\alpha\sigma^6_\eta + \sigma^2_\eta - \frac{\pi S'_0 m^2}{ck} = 0, \quad (38)$$

$$43,65\cdot 10^4 \sigma^6_\eta + \sigma^2_\eta - 187,05\cdot 10^{-5} = 0 . \quad (39)$$

Finally, we have:

$$\sigma^2_\eta = 117\cdot 10^{-5} m^2 . \quad (40)$$

In this case, the coefficient p_e can be expressed

$$p_e^2 = p^2(1 + 15\alpha\sigma_\eta^4) = 15,21 s^{-2} . \quad (41)$$

The velocity variance is given by:

$$\sigma^2_{\dot{\eta}} = \frac{S'_0 \pi m}{c} = 0,27\frac{m^2}{s^2} . \quad (42)$$

The absolute acceleration is given by:

$$\sigma^2_{\ddot{\eta}_{abs}} = \pi S'_0 \left(\frac{c}{m} + \frac{mp_e^2}{c} \right) = 10,42\frac{m^2}{s^4} . \quad (43)$$

It can be seen from (29) that the variance of absolute acceleration increases as the stiffness increases and decreases as the mass increases. As for the effect of damping, it can be shown by taking the derivative of (29) with respective to

$$\frac{\partial\sigma^2_{\ddot{\eta}_{abs}}}{\partial c} = \pi S'_0 \left(\frac{1}{m} - \frac{mp_e^2}{c^2} \right) > 0, \text{ when } c > mp_e \quad (44)$$

$$\frac{\partial\sigma^2_{\ddot{\eta}_{abs}}}{\partial c} = \pi S'_0 \left(\frac{1}{m} - \frac{mp_e^2}{c^2} \right) < 0, \text{ when } c < mp_e \quad (45)$$

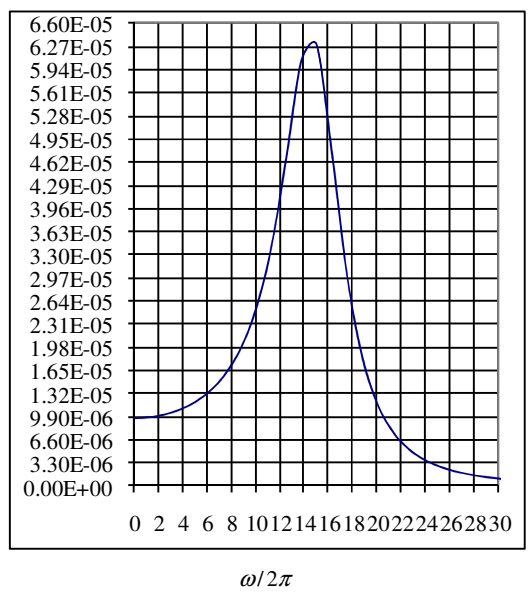

Fig. 2. The power spectral density of response for $\alpha = 3m^{-4}$.

4. REMARKS

This suggests that the variance of absolute acceleration decreases as the damping increases when the damping ratio is smaller than $0,5$. The

variance increases as the damping increases when the damping ratio is bigger than $0,5$ .It can be seen that stiffening structure (increase stiffness) can reduce displacement but would result in the increase of absolute acceleration. On the other hand, increasing mass can reduce absolute acceleration but increase displacement. It seems that the only damping increase (when $\xi < 0,5$) can result in the simultaneous reduction of displacement and absolute acceleration. These conclusions are very useful when designing structure under seismic condition.

REFERENCES

[1] Pandrea, N., Parlac, S.,-*Mechanical vibrations,* Pitesti University, (2000).

[2] Munteanu, M., *Introduction to dinamics oscilation of a rigid body and of a rigid bodies sistems,* Clusium, Cluj Napoca, 1997

[3] Clough, R., W., Penzien, J., *Dynamics of Structures,* McGraw-Hill, New York, (1993).

[4] Zhu, W.,Q., *Stochastic averaging method in random vibration,* Bulletin S.F.M, 5(1988)

[5] Zhu, W.,Q., *Equivalent nonlinear system method for Stochastically excited and dissipated integrable Hamiltonian systems*, Bulletin S.F.M., 7(1997).

[6] Roberts, J.B., Spanos, P.D., *Stochastic averaging:an approximate method of solving random vibration problems*, Int. J. Non-Linear Mech. ,21(1986).

RANDOM VIBRATION OF STRONGLY NON-LINEAR OSCILLATORS

Petre STAN[1], Marinică STAN[2]

[1]METALLURGICAL HIGH SCHOOL, Slatina, Romania.
[2]UNIVERSITY OF PITEŞTI, Romania.

Rezumat. Sistemele puternic neliniare care fac obiectul excitaţiilor aleatoare sunt adesea întâlnite în ştiinţă şi inginerie. O abordare versatilă şi cu bune rezultate aproximative a problemelor de vibraţii aleatoare cu grad puternic de este metoda de liniarizare statistică a ecuaţiilor de mişcare. Metoda se aplică pentru a determina răspunsul la oscilatori neliniari de tip Duffing-van der Pol supuşi la excitaţii externe de bandă largă. Prin urmare, este necesar să se înlocuiască sistemul neliniar cu un sistem liniar echivalent. Metoda de liniarizare se poate folosi pe scară largă în nenumărate probleme inginereşti. Metoda de liniarizare statistică constă în aproximarea unui sistem neliniar cu un sistem liniar, cu anumite condiţii impuse sistemului liniar. În cadrul acestei lucrări se va prezenta o metodă de determinare a densităţii spectrale de putere a răspunsului sistemului oscilator asupra căruia se aplică excitatii aleatoare de bandă largă.
Cuvinte cheie: excitaţie aleatoare, liniarizare echivalentă, densitate spectrală de putere.

Abstract. Strongly non-linear systems subject to random excitation are often met in science and engineering. A versatile and powerful approximate approach to random vibration problems of strongly non-linear systems is the equivalent linearization method. The procedure is applied to predict the response of Duffing-van der Pol oscillator under both external excitations of wide-band stationary random processes. Therefore, it is necessary to replace the nonlinear system with an equivalent linear system. Method of equivalent linearization has been extensively used in these engineering applications. Equivalent linearization method, a nonlinear system can be approximated as a time dependent linear system. By comparing the information of the time-varying natural frequency coefficient between the healthy system and the damaged system, the introduced damage can be identified at a particular time. We present a method for estimating the power spectral density of the stationary response ofstrongly non-linear oscillator with a nonlinear restoring force under external stochastic wide-band excitation.
Keywords: random excitation, equivalent linearization, power spectral density.

1. SISTEM MODEL

To illustrate the procedure of equivalent linearization theory [1], let us consider the following oscillator with a nonlinear restoring force component. The ordinary differential equation of the motion can be written as:

$$m\ddot{\eta}(t) + c\dot{\eta}(t) + g(\eta(t)) = F(t)\,, \qquad (1)$$

where m is the mass, c is the viscous damping coefficient, $F(t)$ is the external excitation signal with zero mean and $\eta(t)$ is the displacement response of the system.

Dividing the equation by m , the equation of motion can be rewritten as:

$$\ddot{\eta}(t) + 2\xi p\dot{\eta}(t) + h(\eta(t)) = f(t)\,, \qquad (2)$$

where ξ is the critical damping factor, and p is the undamped natural frequency, for the linear system.

We can always find a way to decompose the nonlinear restoring force to one linear component plus a nonlinear component

$$h(\eta) = p^2(\eta + G(\eta)\alpha)\,, \qquad (3)$$

where α is the nonlinear factor to control the type and degree of nonlinearity in the system. The idea of linearization [4,5] is replacing the equation by a linear system:

$$\ddot{\eta}(t) + 2\xi_e p_e\dot{\eta}(t) + p_e{}^2\eta(t) = f(t), \qquad (4)$$

where

$$\xi_e = \frac{p}{p_e}\xi \qquad (5)$$

is the damping ratio of equivalent linearized system and p_e is the natural frequency of the equivalent linearized system.

To find an expression for p_e, it is necessary to minimize [2,3] the expected value of the difference between equations (2) and (4) in a least square sense. Now the difference is the difference between the nonlinear stiffness and linear stiffness terms , which is

$$e = h(\eta(t)) - p_e^2 \eta(t) \tag{6}$$

The value of p_e can be obtained by minimizing the expectation , of the square error:

$$\frac{dE\{e^2\}}{dp_e^2} = 0 . \tag{7}$$

The expression of p_e is:

$$p_e^2 = p^2 (1 + \alpha \frac{E\{\eta G(\eta)\}}{\sigma_\eta^2}), \tag{8}$$

where σ_η is the standard deviation of $\eta(t)$. This equation shows how the nonlinear component of the stiffness element affects the value of p_e.

The displacement variance [4,6] of the syste under Gaussian white noise excitation can be expressed as,

$$\sigma_\eta^2 = R_\eta(0) = \int_{-\infty}^{\infty} \left| H(\omega) \right|^2 S_F d\omega, \tag{9}$$

where the frequency response function [5,6] of the single degree of freedom (SDOF) system is,

$$\left| H(\omega) \right| = \frac{1}{m\sqrt{(p_e^2 - \omega^2)^2 + 4\xi_e^2 p_e^2 \omega^2}} . \tag{10}$$

In equation (8), the exact evaluation of $\frac{E\{\eta G(\eta)\}}{\sigma_\eta^2}$ requires knowledge of the first-order density function of the response process $\eta(t)$.

Remark:

For $G(\eta) = 0$, obtain the linear case:

$$p_e = p, \xi_e = \xi, \alpha = 0. \tag{11}$$

2. EXAMPLE: THE RANDOM DUFFING OSCILLATOR

To illustrate the procedure, let us consider the following oscillator with a nonlinear restoring force component.

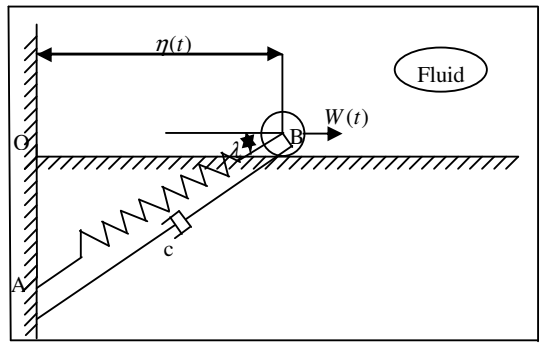

Fig. 1. Spectral analysis of system under random load.

If the distance OA is equal with $d > l_0$, the motion equation is

$$m\ddot{\eta}(t) + c\dot{\eta}(t) + F_r + F\cos\lambda = W(t), \tag{12}$$

where $W(t)$ is the external excitation signal with zero mean and $\eta(t)$ is the displacement response of the system, F_r is the resistence force [4] met in its movement in the liquid, proportional with the liquid viscosity γ, with the representative lenght of the body l and its velocity v, $F_r = K\gamma l v$. For a sferic body

$$K = 6\pi, l = r, \tag{13}$$

so

$$F_r = 6\pi r \gamma v . \tag{14}$$

Becouse

$$F = k(AB - l_0), \tag{15}$$

$$OB = AB\cos\lambda, \tag{16}$$

$$\cos\lambda = \frac{\eta}{\sqrt{d^2 + \eta^2}}, \tag{17}$$

$$p^2 = \frac{k}{m}, \tag{18}$$

result

$$m\ddot{\eta}(t) + c\dot{\eta}(t) + k\left(1 - \frac{l_0}{\sqrt{d^2 + \eta^2}}\right)\eta(t) = 0 . \tag{19}$$

The Fourier Transform is a generalization of the Fourier series. Strictly speaking it applies to continuous and aperiodic functions, but the use of the impulse function allows the use of discrete signals. The set of conditions that guarantee the existence of the Fourier transform is the Dirichlet conditions, which may be expressed as:

1. The signal $\eta(t)$ has a finite number of finite discontinuities.
2. The signal $\eta(t)$ contains a finite number of maxima and minima.
3. The signal $\eta(t)$ is absolutely integrable, that is

$$\int_{-\infty}^{\infty} |\eta(t)| dt < \infty . \qquad (20)$$

We aplicate

$$\frac{\eta}{\sqrt{d^2+\eta^2}} = \frac{1}{d}\left(1+\frac{\eta^2}{d^2}\right)^{-\frac{1}{2}} + \frac{1}{d}\left(1-\frac{\eta^2}{2d^2}+\frac{3\eta^4}{8d^4}+...\right). \qquad (21)$$

Obtain the equation

$$\ddot{\eta}(\tau)+\left(2\xi p+6\pi r\frac{\gamma}{m}\right)\dot{\eta}(\tau)+ +p^2\left(1-\frac{l_0}{d}\right)\eta(t)+p^2\frac{l_0}{2d^3}\eta^3(\tau)- , \qquad (22)$$
$$-p^2\frac{3l_0}{8d^5}\eta^5(\tau)=w(t).$$

where $\xi=\frac{c}{2pm}$ is the critical damping factor, w(t) is the standard Gaussian white noise.
The equation of motion is

$$\ddot{\eta}(t)+\left(2\xi p+6\pi r\mu\right)\dot{\eta}(t)+ +\left[p^2\left(1-\frac{l_0}{d}\right)+3p^2\frac{l_0}{2d^3}\sigma^2{}_\eta\right]\eta(t)=w(t). \qquad (23)$$

The variance of the process $W(t)$ is

$$\sigma^2{}_\eta = \frac{\pi S_0}{2mp^2\left(\xi p+3\pi r\mu\right)\left[\left(1-\frac{l_0}{d}\right)+\frac{3l_0}{2d^3}\sigma^2{}_\eta-\frac{45l_0}{8d^5}\sigma^4{}_\eta\right]}, \qquad (24)$$

or

$$\sigma^2{}_\eta = \frac{\frac{\pi S_0}{p^2}}{\left(c+6\pi r\gamma\right)\left[\left(1-\frac{l_0}{d}\right)+\frac{3l_0}{2d^3}\sigma^2{}_\eta-\frac{45l_0}{8d^5}\sigma^4{}_\eta\right]}. \qquad (25)$$

For

$m=1kg,\ d=1m, k=16\frac{N}{m}, c=1,5, l_0=0,5m, r=6\cdot 10^{-2}m,$

we obtain

$$\sigma^2{}_\eta = \frac{0,65\pi}{\left(1,5+0,0157\right)(8+12\sigma^2{}_\eta-45\sigma^4{}_\eta)}, \qquad (26)$$

or

$$45\sigma^6{}_\eta-12\sigma^4{}_\eta-8\sigma^2{}_\eta+130=0, \qquad (27)$$

with solutions

$$\sigma^2{}_\eta=0,15. \qquad (28)$$

The standard deviation of vellocity is

$$\sigma^2{}_{\dot{\eta}} = \frac{\pi S_0}{m\left(2\xi p+6\pi r\mu\right)} = \frac{\pi S_0}{c+6\pi r\gamma}. \qquad (29)$$

We obtain

$$\sigma^2{}_{\dot{\eta}} = 1,34\frac{m^2}{s^2}. \qquad (30)$$

The natural frequency of the equivalent linearized [6,7] system is

$$p_e{}^2 = p^2\left[\left(1-\frac{l_0}{d}\right)+3\frac{l_0}{2d^3}\sigma^2{}_\eta-\frac{45l_0}{8d^5}\sigma^4{}_\eta\right], \qquad (31)$$

or

$$p_e{}^2 = p^2\left(\frac{1}{2}+\frac{3}{4}\sigma^2{}_\eta-\frac{45}{16}\sigma^4{}_\eta\right)=2,96s^{-1}. \qquad (32)$$

The power spectral density of response is

$$S_\eta(\omega)=\frac{S_F}{m^2}\frac{1}{u^2+4\omega^2(\xi p+3\pi r\mu)^2}, \qquad (33)$$

with

$$u=p^2\left\{\left(1-\frac{l_0}{d}\right)+3p^2\frac{l_0}{2d^3}\sigma^2{}_\eta-\frac{45l_0}{8d^5}\sigma^4{}_\eta\right\}-\omega^2. \qquad (34)$$

We obtain

$$S_\eta(\omega)=\frac{2S_0}{\left\{p^2\left(\frac{1}{2}+\frac{3}{4}\sigma^2{}_\eta-\frac{45}{16}\sigma^4{}_\eta\right)-\omega^2\right\}^2+2,28\omega^2} = \qquad (35)$$
$$=\frac{0,65}{(8,78-\omega)^2+2,28\omega^2}.$$

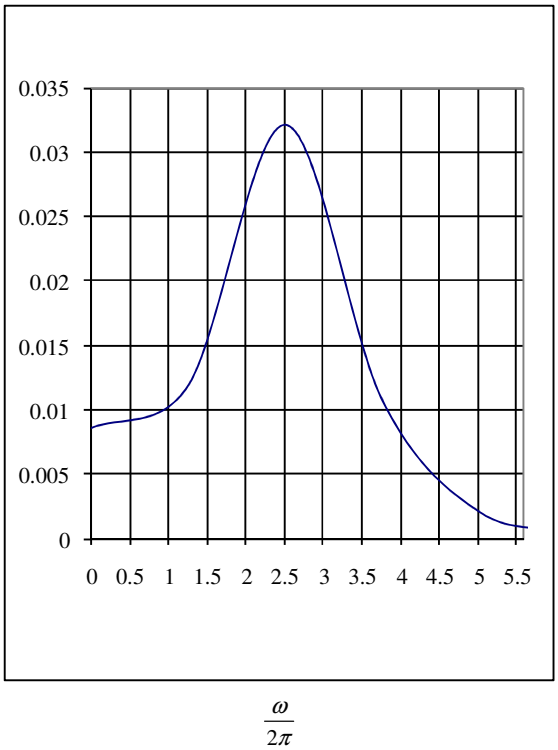

Fig. 2. The power spectral density of response $S_\eta\ [m^2 \cdot s]$ for the power spectral density of excitation $S_F = 0,65 N^2 \cdot s$ and $\gamma = 1,393 \cdot 10^{-2} \frac{kg}{m \cdot s}$.

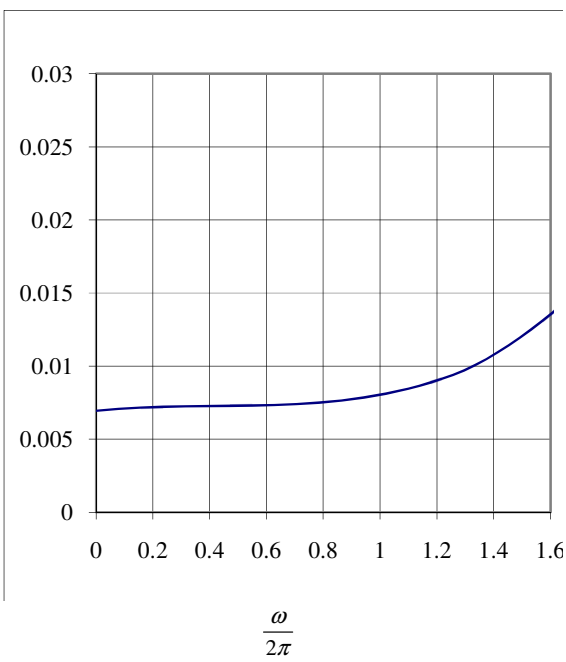

Fig. 3. The power spectral density of response $S_\eta\ [m^2 \cdot s]$ for the power spectral density of excitation $S_F = 0,65 N^2 \cdot s$ and $\gamma = 1,393 \cdot 10^{-2} \frac{kg}{m \cdot s}$ of the hight nonlinearity oscillator system in a small range of frequencies.

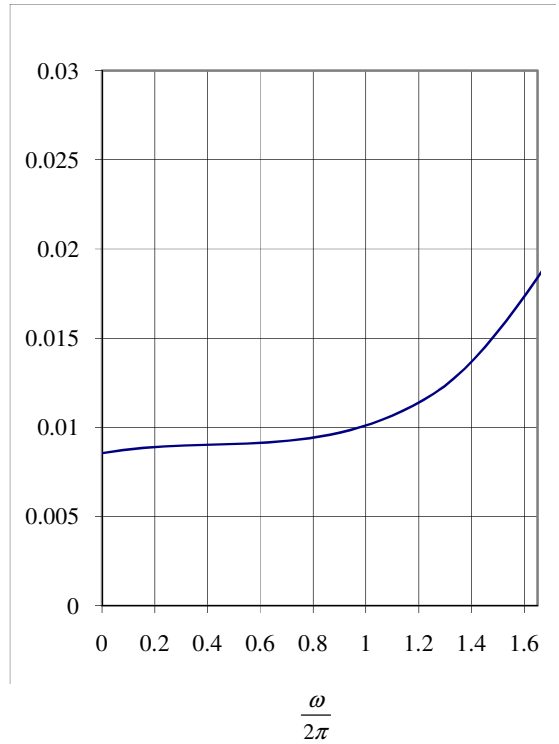

Fig. 4. The power spectral density of response $S_\eta\ [m^2 \cdot s]$ for the power spectral density of excitation $S_F = 0,65 N^2 \cdot s$ and $\gamma = 1,393 \cdot 10^{-2} \frac{kg}{m \cdot s}$ of low hight nonlinearity oscillator system in a small range of frequencies.

3. CONCLUSION

In this article, we are analyzing a differential equation with random variable. Our new technique based on the combination of the transformation method with equivalent linearization theory and minimizing the expectation of the square error to evaluate the probability density function and the power spectral density of the solution.

The accuracy of the procedure depends on the bandwidth of the excitation and of the way to decompose the nonlinear restoring force in one linear component plus a nonlinear component.

Exact solutions for a non-linear system under random excitation are rare. It is known that even under ideal white noise excitation, only for certain types of non-linear systems, the exact probability density function of the response in the steady state can be obtained [7].

Usually the power spectral density of the input is non-white and the probability density function is taken to be Gaussian to seek an approximate solution through equivalent linearization techniques.

The spectral density is approximately constant value of 0.0085 for frequencies between 0 to 0.4

Hz. Maximum power spectral density is 0.032, with a high accuracy solution for the elastic component has a high degree of nonlinearity. Also observing the decrise of pulsation at the rize of viscosity.

Efficient equivalent linear systems with random coefficients for approximating the power spectral density can be deduced.

The resonant peak is described very satisfactorily by the approximate solution

REFERENCES

[1] Pandrea, N., Parlac, S., *Mechanical vibrations*, Pitesti University, 2000.

[2] Munteanu, M., *Introduction to dinamics oscilation of a rigid body and of a rigid bodies sistems*, Clusium, Cluj Napoca, 1997

[3] Zhao, L., Chen, Q., *Equivalent linearization for nonlinear random vibration,* Probabilistic Engineering Mechanics, 9(1993).

[4] Manohar, C.S., Srinivas, Ch., *Nonlinear systems under random differential support motion:response analysis and development of critical excitation models, Earthquake Engineering and Structural dynamics*, 24(1995)

[5] Zhu, W.,Q., *Stochastic averaging method in random vibration,* Bulletin S.F.M, 5(1988)

[6] Zhu, W.,Q., *Equivalent nonlinear system method for Stochastically excited and dissipated integrable Hamiltonian systems*, Bulletin S.F.M., 7(1997).

[7] Roberts, J.B., Spanos, P.D., *Stochastic averaging:an approximate method of solving random vibration problems,* Int. J. Non-Linear Mech. ,21(1986).

METHODS FOR SOLVING COLD OR BACK END CORROSION

Nicusor VATACHI, Viorel POPA

UNIVERSITY "DUNĂREA DE JOS" from Galaţi, Romania

Rezumat: De fiecare dată când combustibili care conţin sulf sunt arşi în cuptoare sau cazane, se formează dioxid de sulf şi într-o măsură mai mică trioxid de sulf, alături de CO_2 şi vapori de apă. Dacă gazele de ardere sunt răcite sub punctul de rouă, CO_2 se poate combina cu vaporii de apă formând acid carbonic, care, deşi slab, poate ataca oţelurile moi. În timp ce eficienţa termică a echipamentului creşte cu reducerea temperaturii (sau entalpiei) de evacuare a gazelor, temperaturile mai mici decât punctul de rouă acidă nu sunt recomandabile pentru suprafeţele metalice în contact cu gazele. În plus faţă de acid sulfuric, pot apărea acid clorhidric şi acid bromic. Acest articol prezintă o metodă de rezolvare a coroziunii acide de joasă temperatură la echipamentele cel mai des folosite la recuperarea căldurii şi anume economizoarele sau preîncălzitoarele de apă.
Cuvinte cheie: cazane, temperatură de evacuare, coroziune de joasă temperatură.

Abstract: Every time when containing sulfur fuels are fired in heaters or boilers, sulfur dioxide, and to a small extent sulfur trioxide, are formed in addition to CO_2 and water vapor. Also, when cooled below the water vapor dew point, CO_2 can combine with water vapor to form carbonic acid, which though weak, can attack mild steel. While thermal efficiency of the equipment is increased with reduction in exit gas temperature (or enthalpy), lower temperatures than the acid gas dew point are not advisable for metallic surfaces in contact with the gas. In addition to sulfuric acid should be existing hydrochloric and hydro bromic acid. This article deals with methods for solving cold, or back end corrosion with the most commonly used heat recovery equipment, namely economizers or water preheaters.
Keywords*:* boilers, exit gas temperature, cold or back end corrosion.

1. INTRODUCTION

When sulfur contained in the fuel is combusted it forms primarily sulfur dioxide. About 2 - 5 % of the sulfur dioxide formed is further oxidized to sulfur trioxide in the presence of appropriate catalysts and additional oxygen. This formation occurs when the dioxide is in contact with an iron or vanadium oxide (slag) surface at temperatures of 500 - 600° C , and if there is extra oxygen in the flue gases to react with it. The trioxide that forms in the flame quickly decomposes back to the dioxide due to thermodynamic considerations. Most of the sulfur trioxide forms after the flame. When sulfur trioxide is present it will condense with water vapor to form sulfuric acid when the acid dew point is reached. This acid collects on iron surfaces causing corrosion. Because the acid dew point will only be reached in colder parts of the boiler this is called **cold-end corrosion**.

Virtually no sulfur trioxide is formed in a boiler except by the above reaction utilizing a catalyst. Unfortunately for the boiler operator the catalyst can be any iron or slag-covered surface at the appropriate temperature. The temperature range at which this occurs is in the range of many boiler superheater and reheater sections. Therefore, almost any boiler that burns a sulfur-containing fuel will generate varying quantities of sulfur trioxide. If the temperature in any part of the boiler drops below the acid dew point (which can be any temperature below about 150°C, depending on the concentration of sulfur trioxide in the flue gas), the sulfur trioxide can condense with water vapor to form highly corrosive sulfuric acid.

Every time when containing sulfur are fired in heaters or boilers, sulfur dioxide, and to a small extent sulfur trioxide, are formed in addition to CO_2 and water vapor. Also, when cooled below the water vapor dew point, CO_2 can combine with water vapor to form carbonic acid, which though weak, can attack mild steel. While thermal efficiency of the equipment is increased with reduction in exit gas temperature (or enthalpy), lower temperatures than the acid gas dew point are not advisable for metallic surfaces in contact with

the gas. In addition to sulfuric acid should be existing hydrochloric and hydro bromic acid.

This article deals with methods for solving cold, or back end corrosion with the most commonly used heat recovery equipment, namely economizers or water preheaters. These are used to preheat feed water entering the system (Fig. 1) and operate at low metal temperatures, thereby increasing their susceptibility to corrosion by sulfuric and carbonic

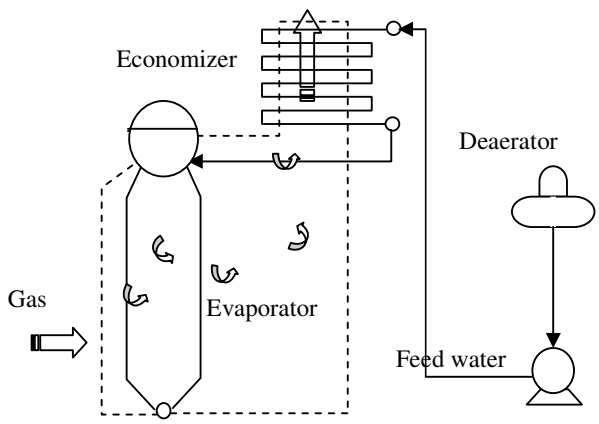

Fig. 1.

acid.

Estimating the dew point of these acid gases is the starting point in understanding the problem of back end corrosion.

The dew points of the various acid gases as a function of their partial pressures in the flue gas are [1],[2],[3]:

- Hydrobromic acid:

$$1/T_{DP} = 3.5639 - 0.1350 \ln(p_{H20}) - 0.0398 \ln(p_{HBr}) + 0.00235 \ln(p_{H20}) \ln(p_{HBr}) \quad (1)$$

- Hydrochloric acid:

$$1/T_{DP} = 3.7368 - 0.1591 \ln(p_{H20}) - 0.0326 \ln(p_{HCl}) + 0.00269 \ln(p_{H20}) \ln(p_{HCl}) \quad (2)$$

- Nitric acid:

$$1/T_{DP} = 3.6614 - 0.1446 \ln(p_{H}) \quad (3)$$

- Sulfurous acid:

$$1/T_{DP} = 3.9526 - 0.1863 \ln(p_{H20}) + 0.000867 \ln(p_{SO2}) - 0.000913 \ln(p_{H20}) \ln(p_{SO2}) \quad (4)$$

- Sulfuric acid:

$$1/T_{DP} = 2.276 - 0.0294 \ln(p_{H20}) - 0.0858 \ln(p_{H2SO4}) + 0.0062 \ln(p_{H20}) \ln(p_{H2SO4}), \quad (5)$$

when T_{DP} is dew point temperature [K] and p [mmHg] is partial pressure.

To compute **the sulfuric acid dew point**, one should know the amount of SO_3 in the flue gases. The formation of SO_3 is primarily derived from two sources.

1. *Reaction of SO_2 with atomic oxygen in the flame zone.* It depends on the excess air used and the sulfur content.
2. *Catalytic oxidation of SO_2* with the oxides of vanadium and iron, which are formed from the vanadium in the fuel oil.

Generally, only 1 to 5 % of SO_2 converts to $S0_3$. For example from 32 ppm SO_2 only 4 ppm would be converted, assuming a 2 % conversion. Using these numbers and after proper conversion and substitution in the equations in equations (1) to (5), we have: dew point of sulfuric acid = 130° C, dew point of hydrochloric acid = 53,3°C, dew point of hydrobromic acid = 56,67°C and dew point of water vapor = 49,44°C. Hence, it is apparent the limiting dew point is that due to sulfuric acid and any heat transfer surface should be above this temperature (130°C) if condensation is to be avoided.

The metal temperature of surfaces such as economizers is not dictates from the gas temperature. To explain this, an example will be worked to show the metal temperature of an economizer with two different gas temperatures:

- when the temperature of gas outside tubes is t_g=399°C average tube wall temperature is 126 °C;
- when the temperature of gas outside tubes is t_g=176°C average tube wall temperature is 122 °C;

It can be seen that the water side coefficient is so high that the tube wall temperature runs very close to the water temperature in spite of a large difference in the gas temperatures. Thus, the tube wall temperature will be close to the water temperature and the water temperature fix the wall temperature and hence, the dew point. Some engineers think that by increasing the flue gas temperature the economizer corrosion can be solved

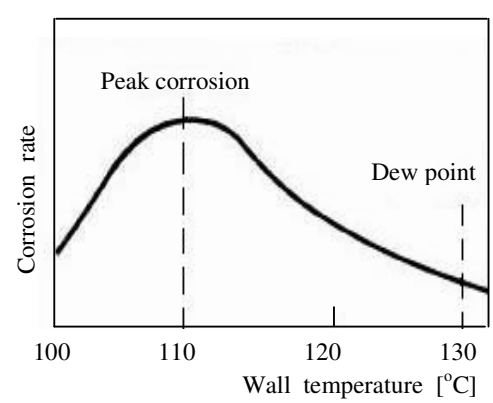

Fig. 2. Corrosion rate as a function of wall temperature

but is not so. It should be noted also that the

maximum corrosion rate occurs at a temperature much below the dew point (Fig. 2).

2. METHODS OF DEALING WITH COLD END CORROSION

To combat the problem of cold end corrosion are two approaches methods:

A). Using protective measures such as maintaining a high cold end temperature so that condensation of any vapor does not occur.

B). Permit condensation of acid vapor or both acid and water vapor, thereby increasing the duty of the heat transfer surface, and use corrosion resistant materials such as glass, teflon, etc.

3. METHODS OF AVOIDING COLD END CORROSION

1). Maintain a reasonably high feed water inlet temperature. If the computed dew point is say 121°C, a feed water of 121°C should keep the minimum tube wall temperature above the dew point. With finned heat transfer surfaces, the wall temperature will be slightly higher than with bare tubes.

The simplest way would be to operate the deaerator at a slightly higher pressure, if the feed water enters the economizer from a deaerator (Fig.1). At 0,35 bar the saturation is 109°C and at 0,7 Bar it is 115°C.

2). In case the deaerator pressure cannot be raised, a heat exchanger may be used ahead of the

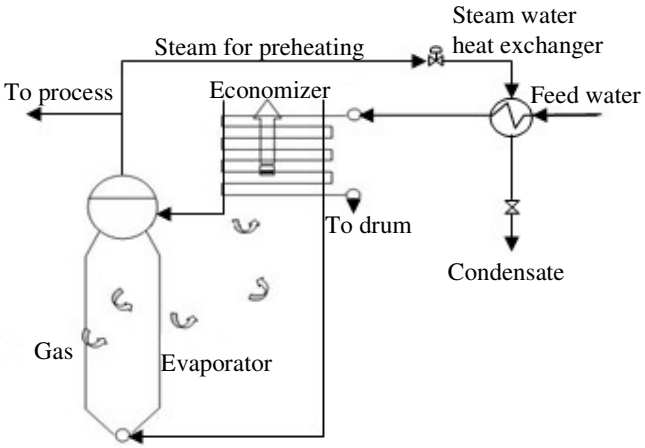

Fig. 3. Steam water exchanger preheats feed water

economizer (Fig. 3) to increase the feed water temperature. It may be steam or water heated.

3). Fig. 4 shows a method for using an exchanger to pre heat the water.

The same amount of water from the economizer exit preheats the incoming water.

By controlling the flow of the hotter water, one can adjust the water temperature to the economizer so that a balance between corrosion criterion and efficiency of operation can be maintained.

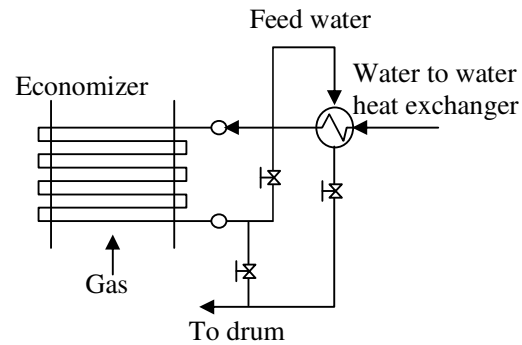

Fig. 4. Water-to-water exchanger preheats feed water

4). Hot water from either the economizer exit or the steam drum (Fig. 5), can be recirculated and mixed with the incoming water. The economizer has to handle a higher flow, but the

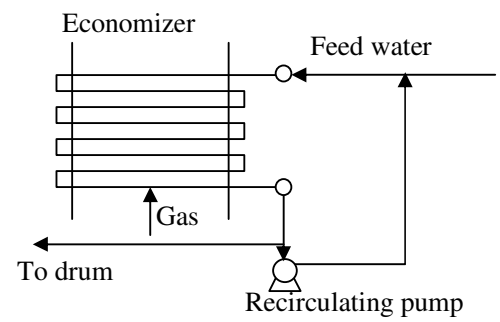

Fig. 5. Recirculating pump mixes hot water with feed water

exchanger is eliminated and a pump is added.

Note that some engineers have the misconception that bypassing a portion of the economizer (Fig. 6) would solve the problem; not so. While bypassing, the heat transfer surface reduces the duty on the economizer and increases the exit gas temperature; it does not help to increase the wall temperature of the tubes, which is the most important variable. A higher exit gas temperature probably helps the downstream ductwork and equipment, but not the economizer. One benefit, however, from bypassing is permitting condensation on surfaces. By using proper materials one can protect the heating surfaces from corrosion attack, if condensation is likely. This concept has now been extended to recovering the sensible and latent heat

from the flue gases, thereby increasing the thermal points in what are called condensing heat exchangers.

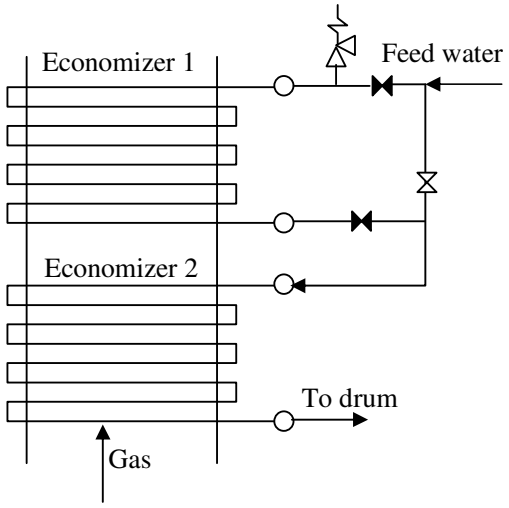

Fig. 6. Bypass arrangement for economizer: Economizer one is bypassed and this increases exit gas temperature and avoids steaming but not dew point corrosion in economizer two.

A large amount of sensible and latent heat in the flue gas can be recovered if the gas is cooled below the water dew point. This implies that sulfuric acid, if present in the gas stream, will condense on the heat transfer surfaces as its dew point is much higher than that of water vapor. Borosilicate glass and teflon coated tubes have been widely used as heat transfer surfaces for this service. Glass is suitable for low pressures and temperatures (less than 232°C and 1,37 to 7 bar). However, presence of fluorides and alkalis is harmful to the glass tubes. One manufacturer of condensing heat exchangers uses teflon coated tubes. A thin film (about 0.015 m.) is extruded onto carbon or alloy steel tubes, and the surface is resistant to corrosion of sulfuric acid.

Hence, these exchangers will be larger than those with extended surfaces, however, the higher heat transfer rates with condensation process improves the overall heat transfer coefficients and partly compensates for the lower surface area per linear foot of bare tubes.

efficiency of the system by several percentage

The high initial investment associated with condensing heat exchangers has to be carefully reviewed along with the energy recovered, fuel costs, etc. If the fuel cost is not high, then the payback period for this type of equipment may be long.

Materials such as cast iron and stainless steels probably have better corrosion resistance than carbon steel, but still they are not.

4. CONCLUSION

The article outlined the importance of the dew point of acid gas and methods for dealing with the problem of condensation on heating surfaces such as economizers. Similar methods could be used for air heaters. The basic difference lies in the fact that the back end temperature is a function of both the gas and air temperatures. Steam air heating or air bypassing have been used to combat the problem of corrosion.

Replaceable matrices and corrosion resistant materials such as enamels have been used at the cold end of regenerative air beaters.

REFERENCES

[1]. Perry, R. H., and Chilton C. H., ed., *"Chemical Engineers'Handbook",* 5th ed., McGraw-Hill, New York, 1973.

[2]. Pierce, R. R., *"Estimating acid dewpoints in stack gases",* Chem.Eng., Apt. 11, 1973.

[3]. Ganapathy, V., *"Nomograms for steam generation and utilization"* ,Fairmont Press, 1986, p. 15.

[4]. Kiang, Yen-Hsiung, *"Predicting dewpoints of acid gases"* ,Chemical Engineering, Feb. 9, 1981, p. 127.

[5]. Vatachi, Nicuşor., *"The experimental determination of steam boilers flue gas dew temperature",* Eight International Expert Meeting Power Engineering 1999, Maribor, Slovenia, Proceedings, pp.191-201.

[6]. Vatachi, Nicuşor., *"The dynamics control of steam boiler pressure and the dew temperature",* Communications Scientifiques Du 1er Symposium International Euretech, 16/17 Juillet, 1999, Settat, Maroc, Partie Roumaine, Tome 1, Pag. 9-10.

[7]. Verhoff, F H., and Banchero, J. T, *"Predicting Dew Points of Flue Gases*," Chem. Eng. Prog., August, 1974.